Published in final edited form as:
J Am Chem Soc. 2012 November 14; 134(45): 18843–18852. doi:10.1021/ja309216v.

Synthetic Models for the [FeFe]-Hydrogenase: Catalytic Proton Reduction and the Structure of the Doubly Protonated Intermediate

Maria E. Carroll,
School of Chemical Sciences, University of Illinois at Urbana-Champaign, Urbana, IL 61801

Bryan E. Barton,
School of Chemical Sciences, University of Illinois at Urbana-Champaign, Urbana, IL 61801

Thomas B. Rauchfuss*, and
School of Chemical Sciences, University of Illinois at Urbana-Champaign, Urbana, IL 61801

Patrick J. Carroll
Department of Chemistry, University of Pennsylvania, Philadelphia, PA

Abstract

This report compares biomimetic HER catalysts with and without the amine cofactor (adt^{NH}): $Fe_2(adt^{NH})(CO)_2(dppv)_2$ (**1**^{NH}) and $Fe_2(pdt)(CO)_2(dppv)_2$ (**2**; $(adt^{NH})^{2-}$ = $(HN(CH_2S)_2^{2-}$, pdt^{2-} = 1,3-$(CH_2)_3S_2^{2-}$). These compounds are spectroscopically, structurally, and stereodynamically very similar but exhibit very different catalytic properties. Protonation of **1**^{NH} and **2** each give three isomeric hydrides beginning with the kinetically favored terminal hydride, which converts sequentially to *sym* and *unsym* isomers of the bridging hydrides. In the case of the amine, the corresponding ammonium-hydrides are also observed. In the case of the terminal amine hydride [*t*-H**1**^{NH}]BF_4, the ammonium/amine-hydride equilibrium is sensitive to counteranions and solvent. The species [*t*-H**1**^{NH2}]$(BF_4)_2$ represents the first example of a crystallographically characterized terminal hydride produced by protonation. The NH--HFe distance of 1.88(7) Å indicates dihydrogen bonding. The bridging hydrides [μ-H**1**^{NH}]$^+$ and [μ-H**2**]$^+$ reduce near −1.8 V, about 150 mV more negative than the reductions of the terminal hydride [*t*-H**1**^{NH}]$^+$ and [*t*-H**2**]$^+$ at −1.65 V. Reductions of the amine hydrides [*t*-H**1**^{NH}]$^+$ and [*t*-H**1**^{NH2}]$^{2+}$ are irreversible. For the pdt analog, the [*t*-H**2**]$^{+/0}$ couple is unaffected by weak acids (pK_a^{MeCN} 15.3) but exhibits catalysis with HBF_4•Et_2O, albeit with a TOF around 4 s^{-1} and an overpotential greater than 1 V. The voltammetry of [*t*-H**1**^{NH}]$^+$ is strongly affected by relatively weak acids and proceeds at 5000 s^{-1} with an overpotential of 0.7 V. The ammonium-hydride [*t*-H**1**^{NH2}]$^{2+}$ is a faster catalyst with an estimated TOF of 58,000 s^{-1} and an overpotential of 0.5 V.

Introduction

In nature, hydrogen is primarily produced and oxidized by the hydrogenase (H_2ase) enzymes.[2] For example, under fermentative conditions, organisms release accumulated

Corresponding Author, rauchfuz@illinois.edu.

ASSOCIATED CONTENT

Supporting Information

Results from NMR, IR spectra, X-ray crystallographic, and electrochemical analyses. This material is available free of charge via the Internet at http://pubs.acs.org.

Notes

The authors declare no competing financial interest.

reducing equivalents as H_2. This H_2 can be captured by other organisms, where it is utilized, via hydrogenases, to reduce oxides such as sulfate.[3] These enzymes have attracted attention as proven motifs for the processing of hydrogen.[4,5] A key goal in this area is the elucidation of catalytic mechanisms.

The first step in characterizing catalytic mechanism is understanding the structure of the active sites. Two genetically unrelated H_2ases have been identified, they contain Ni and/or Fe thiolate centers, the latter bound to CN^- and CO, and are generally rich in Fe-S clusters, emphasizing the central role of electron-transfer.[1,6] [FeFe]-H_2ases are more active than [NiFe]-H_2ases, and they more commonly function as catalysts for H_2 production (Table 1).[7] In the case of [FeFe]-H_2ases, one 4Fe-4S cluster is directly tethered to the diiron active site, the 6Fe ensemble being called the H-cluster. The [FeFe]-H_2ases also feature an amino-dithiolate cofactor that bridges the two organoiron centers (Figure 1).[8]

One widely embraced method to mechanistic analysis of the enzymes entails studies on synthetic diiron dithiolato compounds that are structurally similar to the active site.[4,9] This approach benefits from many decades of research on organoFe-S clusters.[10] Indeed, soon after the structure of the enzymes from *C. pasteurianum* and *D. desulfuricans* were reported, the diiron dithiolato dicyanides $[Fe_2(pdt)(CN)_2(CO)_4]^{2-}$ (pdt = 1,3-propandithiolate) were described.[11] These species proved to be not very useful in developing functional models however. Since that time, two simplifications have been particularly enabling. First, tertiary phosphine (and other) ligands are used in place of cyanide (and some CO) ligands found in the natural catalysts.[12] Second, in place of the appended 4Fe-4S cluster, models usually rely on electrodes to supply and accept electrons. No compromise is required for the amine-dithiolate cofactor (adt), which is incorporated into our models without modification.[13]

Consensus from the biophysical[3] and organometallic[4,12] studies points to the intermediacy of iron hydrides in catalytic function of [FeFe]-H_2ase. Although much is known about iron hydrides,[14] our understanding of diiron dithiolato hydride frameworks is still underdeveloped. CO-rich compounds such as $Fe_2(SR)_2(CO)_6$ are only protonated by very strong acids,[15] hence the requirement that some CO ligands be replaced by more basic donors. In almost all hydride derivatives of diiron dithiolates, the hydride ligand bridges the two metals. This geometry resembles that found in the [NiFe]-H_2ases, but biophysical[3] and computational studies[16] on the [FeFe]-H_2ases strongly indicate that the hydride is located at the apical position of a single organoFe center. A number of diiron complexes with terminal hydride ligands have been characterized, although usually only by NMR spectroscopy. The terminal hydride complexes $[HFe_2(pdt)(CO)_4(chel)]^+$ are often observable by NMR spectroscopy, but above ca. −30 °C they isomerize to bridging hydride complexes (chel = chelating ligands).[17,18] The stability of these terminal hydride complexes is enhanced for sterically crowded or very electron-rich diiron dithiolato carbonyls.[1920] Thus, $Fe_2(pdt)(CO)_2(dppv)_2$ (**2**, pdt = 1,3-propanedithiolate) undergoes protonation, albeit only with strong acids, to give a terminal hydride with a half-life of several minutes at room temperature (dppv = *cis*-$C_2H_2(PPh_2)_2$). Additionally, this terminal hydride derivative was shown to reduce at a potential ca. 100 mV less negative than the isomeric bridging hydride complex.[19]

Herein we summarize an extensive investigation of the structural and protonation chemistry of $Fe_2(adt^{NH})(CO)_2(dppv)_2$ (**1^{NH}**) (adt^{NH} = $[(SCH_2)_2NH]^{2-}$), with parallel studies on the $Fe_2(pdt)(CO)_2(dppv)_2$ (**2**), which lacks the amine cofactor. Overall, the results indicate that the combination of a terminal hydride and the azadithiolate cofactor greatly facilitates reduction of protons to form H_2 by diiron complexes. We also describe a rare crystal structure of a terminal hydride of this series of model diiron dithiolato complexes.

Results

Characterization of $Fe_2(adt^{NH})(CO)_2(dppv)_2$

The main catalyst of interest is $Fe_2(adt^{NH})(CO)_2(dppv)_2$ (**1**^{NH}), a greenish-brown, air-sensitive solid that is highly soluble in dichloromethane and toluene. The IR spectra for **1**^{NH} (ν_{CO} = 1888, 1868 cm^{-1}) and related derivatives $Fe_2(pdt)(CO)_2(dppv)_2$ (**2**), $Fe_2(edt)(CO)_2(dppv)_2$, and $Fe_2(odt)(CO)_2(dppv)_2$ are similar, which indicates that they adopt similar structures and that the donor properties of the dithiolates are similar (edt^{2-} = 1,2-$C_2H_4S_2^{2-}$; odt^{2-} = $O(C_2H_4S)_2^{2-}$).[21] Compounds **1**^{NH} and **2** are stereochemically nonrigid in two ways: (i) "turnstile rotation" of the Fe(dppv)(CO) subunits and (ii) "flipping" of the dithiolate bridge. With respect to the latter process, the $X(CH_2S)_2Fe$ rings (X = CH_2, NH, O, etc) are subject to a chair-chair equilibration,[22] as seen in cyclohexane and piperidine derivatives.[23]

At −80 °C, the ^{31}P NMR spectrum of **1**^{NH} displays four equally intense signals indicating that the two dppv ligands are chemically inequivalent. In contrast, spectra for the related pdt complexes show only a pair of signals at low temperatures, an observation that suggests that pdt is a more flexible dithiolate than adt. Turnstile rotation at the Fe(dppv)(CO) unit is halted on the NMR timescale at −80 °C, but flipping of the dithiolate remains fast. In the adt derivative, both processes are either slow or cease to occur at low temperatures, which may reflect a higher barrier for the flipping of the adt compared to the structurally related pdt derivative.* At −10 °C, this conformational equilibrium becomes rapid on the NMR timescale, and the ^{31}P NMR spectrum simplifies to a broad singlet. The dynamics of the adt and the turnstile rotation of the Fe(CO)(dppv) centers appear to be coupled since both processes change from slow to fast exchange regimes at the same temperature range (see Supplementary Information).

The structure of **1**^{NH} was confirmed crystallographically (Figure 2), the details being consistent with the NMR results. Space-filling models show that the phenyl groups protect the Fe-Fe bond, which is relevant to the regiochemistry of the protonation of **1**^{NH} and **2**.

Isomers of $[HFe_2(adt^{NH})(CO)_2(dppv)_2]^+$

Protonation of **1**^{NH} gives three isomeric hydrides as well as ammonium derivatives or combinations of both. Addition of $[H(OEt_2)_2]BAr^F_4$ to a CH_2Cl_2 solution of **1**^{NH} at −80 °C initially afforded the terminal hydride [*t*-$HFe_2(adt^{NH})(CO)_2(dppv)_2]^+$ ([*t*-H**1**^{NH}]$^+$) ($BAr^F_4{}^-$ = $B(3,5\text{-}C_6H_3(CF_3)_2)_4^-$, Scheme 1). Its high field ^{1}H NMR spectrum, a triplet near δ −4.2, indicates a single isomer (Table 2, Figures 2 and 3). Such relatively low field chemical shifts are often associated with terminal hydrides of diiron dithiolates.[17–20] The ^{31}P NMR spectrum, which features four equally intense singlets (Table 2), uniquely defines the structure: the diphosphine on the FeH center is dibasal and the diphosphine on the other ("proximal") Fe center spans apical and basal sites (^{31}P-^{31}P coupling is often weak in such complexes).[24]

The NMR spectrum of [*t*-H**1**^{NH}]$^+$ changes at higher temperatures indicative of interconversion between the Fe-H and ammonium tautomers. Above −20 °C, the triplet at δ −4.2 in the ^{1}H NMR spectrum broadens, as do the ^{31}P NMR signals, consistent with exchange between the hydride and ammonium tautomers (Scheme 2). Near room temperature, [*t*-H**1**^{NH}]$^+$ converts sequentially to two isomers that feature bridging hydride ligands ("μ-hydrides", Scheme 1). The first μ-hydride isomer, *sym*-[μ-H**1**^{NH}]$^+$, has C_2-

The barriers for ring flipping for the $Fe_2(xdt)(CO)_4(dppv)$ (xdt = pdt ($(SCH_2)_2CH_2^{2-}$), odt ($(SCH_2)_2O^{2-}$), and adt ($(SCH_2)_2NH^{2-}$) from DNMR studies (coalescence temperatures, K): pdt 42 (225), odt 43.3 (235), adt 55.9 kj/mol (293). The variation reflects increased stiffness of the two C-N bonds in the adt backbone, as a consequence of the interaction of the amine lone pair and the C-S σ orbitals. M. T. Olsen, unpublished results.

symmetry (ignoring the adt ligand, which is rapidly flexing and hence effectively planar). In *sym*-[μ-H**1**$^{\mathbf{NH}}$]$^+$, each dppv ligand spans one apical and one basal site. Upon re-cooling a solution of *sym*-[μ-H**1**$^{\mathbf{NH}}$]$^+$ to 0 °C, the terminal hydride species does not reform. Within minutes at room temperature, *sym*-[μ-H**1**$^{\mathbf{NH}}$]$^+$ converts to an unsymmetrical isomer labeled *unsym*-[μ-H**1**$^{\mathbf{NH}}$]$^+$. In *unsym*-[μ-H**1**$^{\mathbf{NH}}$]$^+$, one diphosphine remains apical-basal and the other is dibasal as indicated by ^{31}P NMR spectrum, which consists of four singlets. After allowing the solution to stand for 12 h at room temperature, a 1:5 equilibrium distribution is reached, favoring *unsym*-[μ-H**1**$^{\mathbf{NH}}$]$^+$. The isomerization of ([*t*-H**1**$^{\mathbf{NH}}$]$^+$ is similar to that observed for the hydrides of **2**.[18]

Addition of [H(OEt$_2$)$_2$]BAr$^F_4$ to a CH_2Cl_2 solution of [μ-H**1**$^{\mathbf{NH}}$]$^+$ shifts the ν_{CO} pattern about 15 cm^{-1} to higher energy. This change is indicative of *N*-protonation to form the ammonium-hydride [μ-H**1**$^{\mathbf{NH2}}$]$^{2+}$ (Scheme 1).[25] *N*-protonation is also indicated by the ^{1}H NMR signal for the hydride, which shifts to higher field. The symmetrical isomer, *sym*-[μ-H**1**$^{\mathbf{NH2}}$]$^{2+}$, is the major species in solution, in contrast to the situation for [μ-H**2**]$^+$ and [μ-H**1**$^{\mathbf{NH}}$]$^+$.

IR spectroscopic measurements on the protonation reactions are consistent with the sequence of reactions proposed in Scheme 1. The main feature of interest is the ca. 70 cm^{-1} shift in ν_{COavg} upon protonation of **1**$^{\mathbf{NH}}$ by [H(OEt$_2$)$_2$]BAr$^F_4$, regardless of the *t*- vs μ-hydride isomer. IR spectra in the ν_{CO} region also distinguish terminal and bridging hydrides. The terminal hydrides shows two well-resolved bands, ν_{CO} = 1965 and 1915 cm^{-1}, with the band at lower frequency assigned to the semi-bridging CO. The IR spectra of μ-hydrides show two bands, ν_{CO} ~ 1948 and 1969 cm^{-1}.

Protonation of $Fe_2(adt^{NH})(CO)_2(dppv)_2$ with HBF_4•Et_2O

The identity of the acid affects the course of protonation of **1**$^{\mathbf{NH}}$. Thus, treatment of CH_2Cl_2 solutions with HBF_4•Et_2O (vs [H(OEt$_2$)$_2$]BAr$^F_4$ discussed above) afforded not only [*t*-H**1**$^{\mathbf{NH}}$]$^+$ but also a second species. The pattern for the ν_{CO} bands for the other species is identical to that for **1**$^{\mathbf{NH}}$, but the bands are shifted approximately 20 cm^{-1} to higher energy, characteristic of *N*-protonation.[25,26] The new species is thus assigned as the ammonium tautomer ([**1**$^{\mathbf{NH2}}$]$^+$, Schemes 1,2). The formation of the tautomer is attributed to the ability of BF_4^- to participate in hydrogen-bonding (Scheme 2),[27] which has been observed previously in complexes of protonated adt ligands.[28] The ratio [*t*-H**1**$^{\mathbf{NH}}$]$^+$/[**1**$^{\mathbf{NH2}}$]$^+$ increased from 2:1 to approximately 1:1, in the presence of 10 equiv of [Bu_4N]BF_4. Over the course of several minutes at room temperature, the [*t*-H**1**$^{\mathbf{NH}}$]BF_4/[**1**$^{\mathbf{NH2}}$]BF_4 mixture isomerized to the μ-hydrides. Thus, although BF_4^- stabilizes the ammonium tautomer, the mixture isomerizes in the usual way, forming the μ-hydride species.

The [**1**$^{\mathbf{NH2}}$]BF_4/[*t*-H**1**$^{\mathbf{NH}}$]BF_4 ratio is also affected by the solvent.

Diprotonation of $Fe_2(adt^{NH})(CO)_2(dppv)_2$

Relevant to the electrocatalysis discussed below, **1**$^{\mathbf{NH}}$ undergoes double protonation. Addition of *excess* of [H(OEt$_2$)$_2$]BAr$^F_4$, HBF_4•Et_2O, or CF_3CO_2H to a CH_2Cl_2 solution of [*t*-H**1**$^{\mathbf{NH}}$]$^+$ gave a new species assigned as the ammonium-hydride [*t*-H**1**$^{\mathbf{NH2}}$]$^{2+}$ (Figures 3 and 4). According to ^{1}H and ^{31}P NMR spectra, [*t*-H**1**$^{\mathbf{NH2}}$]$^{2+}$ is structurally similar to [*t*-H**1**$^{\mathbf{NH}}$]$^+$, i.e. a single isomer with both dibasal (distal to the hydride) and apical-basal (proximal) diphosphine ligands (Table 2). As seen for **1**$^{\mathbf{NH}}$ vs [**1**$^{\mathbf{NH2}}$]$^+$, *N*-protonation shifts ν_{CO} bands to higher energy by 20 cm^{-1}, compared to that for [*t*-H**1**$^{\mathbf{NH}}$]$^+$.

After attempts over the course of several years, single crystals of an ammonium hydride were obtained in the form of the salt [*t*-H**1**$^{\mathbf{NH2}}$]$(BF_4)_2$ (Figure 5). In the dication, two

Fe(dppv)(CO) centers are linked in the usual way by a dithiolate. One CO ligand is semi-bridging with an Fe-Fe-C and Fe-C-O angles of 66.68(14) and 166.1(4)°, respectively.[29] The dispositions of the dppv groups, being dibasal and apical-basal, conform with the NMR measurements. The crystals are of sufficient quality that the H centers attached to nitrogen and iron were located and refined. Two phenyl groups on the Fe(1)(dppv) center, equivalent to the distal Fe in the active site, form a pocket around the Fe-H and N-H centers. The Fe-H distance of 1.44(4) Å is normal for a ferrous hydride.[30] The ammonium center of the dithiolate cofactor adtH$^+$ is adjacent to the Fe-*H* center. The NH---HFe distance of 1.88(7) Å is shorter than 2.4 Å distance that is twice the van der Waals radius of hydrogen,[31] indicative of dihydrogen bonding.

Protonation of $Fe_2(xdt)(CO)_2(dppv)_2$ (xdt = adt^{NH}, pdt) with Weak Acids

Weak acids that do not convert **1**$^{\mathbf{NH}}$ into detectable levels of [*t*-H**1**$^{\mathbf{NH}}$]$^+$ at low temperatures quantitatively give [μ-H**1**$^{\mathbf{NH}}$]$^+$ near room temperature. Qualitatively, the rate of formation of [μ-H**1**$^{\mathbf{NH}}$]$^+$ correlates with the strength of the acid. Thus, [HNMe$_3$]BAr$^F{}_4$ (pK_a^{MeCN} = 17.6)[32] rapidly converted **1** to [μ-H**1**$^{\mathbf{NH}}$]$^+$, whereas the same conversion using [HNEt$_3$]BF$_4$ (pK_a^{MeCN} = 18.6)[32] required days for full conversion.

Addition of CF_3CO_2H (pK_a^{MeCN} = 12.7)[32] to **1**$^{\mathbf{NH}}$ at −40 °C gave [*t*-H**1**$^{\mathbf{NH2}}$]$^{2+}$. The IR spectrum (ν_{CO} = 1986 and 1950 cm^{-1}) of the trifluoroacetate differs from that (ν_{CO} = 1986 and 1925 cm^{-1}) obtained by protonation with [H(OEt$_2$)$_2$]BAr$^F{}_4$ and HBF$_4$•Et$_2$O, a difference attributed to hydrogen bonding between the trifluoroacetate and the protonated adt ligand. In contrast to the acid-base behavior of **1**$^{\mathbf{NH}}$, the pdt derivative, **2**, is unaffected by weak acids.

Redox Properties of the Protonated Derivatives of $Fe_2(xdt)(CO)_2(dppv)_2$ (xdt = adt^{NH}, pdt)

In CH_2Cl_2 solutions, the μ-hydrides [μ-H**1**$^{\mathbf{NH}}$]$^+$ and [μ-H**2**]$^+$ reversibly reduce near −1.8 V. Reduction of the doubly protonated species [μ-H**1**$^{\mathbf{NH2}}$]$^{2+}$ occurs about ~ 100 mV positive of the [μ-H**1**$^{\mathbf{NH}}$]$^{+/0}$ couple, as observed for other adt-hydrido complexes.[33] The terminal hydrides [*t*-H**1**$^{\mathbf{NH}}$]$^+$ and [*t*-H**2**]$^+$ are redox-active at milder potentials, the pdt derivative [*t*-H**2**]$^+$ reducing quasi-reversibly (i_p/i_c = 1.57) at –1.67 V. Reduction of [*t*-H**2**]$^+$ is a 1e$^-$ process as indicated by the similarity of the dependence of i_p vs $\nu^{1/2}$ for the couples [*t*-H**2**]$^{+/0}$ and [**2**]$^{0/+}$.[19] We have independently established the stoichiometry of the [**2**]$^{0/+}$ couple.[34] The amino-hydride [*t*-H**1**$^{\mathbf{NH}}$]$^+$ reduces at nearly the same potential (−1.64 V), but the couple is *irreversible* in contrast to the [*t*-**2**H]$^{+/0}$ couple. The ammonium hydride [*t*-H**1**$^{\mathbf{NH2}}$]$^{2+}$ also reduces irreversibly but at the mild potential of −1.3 V (Table 3). Although the reduction potential is milder, stronger acids are required to generate this doubly protonated species. Finally, both the [*t*-H**1**$^{\mathbf{NH}}$]$^{+/0}$ and the [*t*-H**2**]$^{+/0}$ proved insensitive to the electrolyte, i.e. [Bu$_4$N]BAr$^F{}_4$ and [Bu$_4$N]PF$_6$.

Proton Reduction Catalysis by $Fe_2(pdt)(CO)_2(dppv)_2$

For comparison with the catalyst that contains the amine cofactor, the catalytic properties of [*t*-H**2**]$^+$ and [μ-H**2**]$^+$ were evaluated. Strong acids such HBF$_4$•Et$_2$O (pK_a^{MeCN} = −3)[35] are required to protonate **2**, readily giving the terminal hydride [*t*-H**2**]$^+$, which is stable for many minutes at 0 °C. The [*t*-H**2**]$^{+/0}$ couple at −1.67 V is partially reversible even at scan rates as slow as 25 mV/s. Addition of $ClCH_2CO_2H$ (pK_a^{MeCN} = 15.3)[35] has no effect on the electrochemical properties of [*t*-H**2**]$^+$. Addition of HBF$_4$•Et$_2$O results in an increase in current for the couple at −1.67 V, indicative of catalysis. The ratio i_c/i_p increases linearly with [H$^+$] up to 8 equiv of acid, indicating a catalytic pathway that is second order with respect to [H$^+$]. Above this level, i_c/i_p reached a plateau near 5. The turnover frequency is calculated to be ~5 s^{-1} (See Supporting Information). The overpotential is estimated to be

1.3 V. Overpotentials represent the difference between the catalytic potential, E_{cat}, and the standard reduction potential of the acid, $E°_{HA/H2}$ (See Table 4).

The catalytic properties of [μ-**2**H]$^+$ were also examined. Addition of $ClCH_2CO_2H$ to a solution of [μ-**2**H]BF_4 results in an increase in the current for the −1.8 V couple (See SI). Plots of i_c/i_p vs [H^+] are linear up to 10 equiv of acid, and the rate of catalysis by this derivative is calculated to be ~3 s^{-1}. The overpotential is estimated to be 0.95 V for this very slow process.[35]

Proton Reduction Catalysis by $Fe_2(adt^{NH})(CO)_2(dppv)_2$

In contrast to the behavior of the pdt complex, the voltammetry of [*t*-H**1**^{NH}]$^+$ is strongly affected by relatively weak acids. Experiments employed [Bu_4N]BAr^F_4 as the electrolyte to maximize the equilibrium concentration of [*t*-H**1**^{NH}]$^+$ vs its tautomer [**1**^{NH2}]$^+$. When [*t*-H**1**^{NH}]$^+$ was generated *in-situ* from **1**^{NH} and one equiv of [$H(OEt_2)_2$]BAr^F_4, the current for the [*t*-H**1**^{NH}]$^{+/0}$ couple closely matched the current for the [**1**^{NH}]$^{0/+}$ couple, indicating that both events correspond to one-electron couples. Whereas the couple [**2**H]$^{+/0}$ is partially reversible, the [*t*-H**1**^{NH}]$^{+/0}$ couple is completely irreversible (Supporting Information). Upon addition of $ClCH_2CO_2H$ to solutions of **1**, the reductive current at −1.64 V sharply increased and i_{pc} shifts to more positive potential (E_{cat} = −1.43 V), indicative of catalytic proton reduction (Figure 6).[35] A plot of i_c/i_p vs [H^+] is linear over the range 50 to 400 equiv. The maximum i_c/i_p of ~70 corresponds to a rate of 5000 s^{-1} (Figure 7). Gas chromatographic analysis showed that a 90% yield of hydrogen was produced by bulk electrolysis.

By the standards of synthetic catalysts, [*t*-H**1**^{NH}]$^+$ is a fast catalyst, but [*t*-H**1**^{NH2}]$^{2+}$ appears to be even faster. Thus, in the presence of strong acids such as $HBF_4·Et_2O$ or trifluoroacetic acid (TFA), a catalytic wave is observed at −1.22 V. This lower potential process is assigned to electrocatalysis by [*t*-H**1**^{NH2}]$^{2+}$, the ammonium-terminal hydride that predominates in the presence of such strong acids. Monitoring the current at −1.2 V, the variation of i_c/i_p vs [TFA] was found to be linear over 20 – 300 equiv. The maximum i_c/i_p of ~167 corresponds to an estimated turnover frequency of 58,000 s^{-1} (Figures 8, 9).

Hydrogen evolution by electrolysis is typically subject to substantial isotope effects,[36] and this aspect was observed with **1**^{NH}. The dependence of the i_c/i_p vs [$ClCH_2CO_2D$] is linear up to 60 equiv of acid, and reaches a plateau at i_c/i_p of 18, which corresponds to a turnover frequency of 420 s^{-1}. The rate decreased ten-fold, compared to that exhibited in experiments that utilize $ClCH_2CO_2H$ (maximum i_c/i_p = 66, k = 4500 s^{-1}). Similarly, when CF_3CO_2D is substituted for CF_3CO_2H, k decreases by about 15%, with the maximum i_c/i_p = 106 and k = 6600 s^{-1}.

Electrocatalysis experiments were conducted with the bridging hydride [μ-H**1**^{NH}]$^+$ also at 0 °C. At −1.8 V, the current increases with the addition of $ClCH_2CO_2H$. A plot of i_c/i_p vs [H^+] is linear over the range 2–50 equiv of $ClCH_2CO_2H$, but begins to plateau at 60 equiv, corresponding to an i_c/i_p of ~10 (Figure 7). The catalytic rate is estimated as 20 s^{-1}. The μ-hydride operates at an overpotential of 0.9 V, which is 0.2–0.4 V higher than the overpotentials for the terminal species.

Conclusions

Hydrogen evolution by biomimetic diiron dithiolates is accelerated by the amine cofactor, to which the hydride ligand must be adjacent. The protonated derivatives of **1**^{NH} and **2** exhibit very different catalytic properties, although the neutral complexes are almost indistinguishable spectroscopically. Thus, the adt and pdt ligands have comparable inductive effects resulting in complexes of very similar thermodynamic properties. The

crystallographic analysis of [*t*-H**1**$^{\mathbf{NH2}}$]$^{2+}$ provides a unique insight into a probable intermediate in both the evolution and oxidation of hydrogen. The specific point of interest is the short distance between the hydride and the proton on the ammonium cofactor. The implied dihydrogen bonding provides a snapshot of a step in the formation and scission of a dihydrogen molecule at the active site of the [FeFe]-H_2ase.

An attractive $NH^{\delta+}$---$H^{\delta-}$ interaction may be relevant to the small separation between the first and second protonation constants, estimated at only 10^2 in CH_2Cl_2 solution. In comparison with [*t*-H**1**$^{\mathbf{NH}}$]$^+$, the [*t*-H**1**$^{\mathbf{NH2}}$]$^{2+}$ isomerizes to the μ-hydride more slowly, which may result from this interaction.

The basicities of two sites - the terminal Fe center and the amine are closely balanced. In CH_2Cl_2 solution, Fe is more basic, but the equilibrium shifts in the presence of hydrogen-bond acceptors as demonstrated with the influence of Bu_4NBF_4 on this equilibrium. The lower basicity of a terminal Fe site vs the Fe-Fe bond is indicated by the conversion of mixtures of ammonium cations and **1**$^{\mathbf{NH}}$ into [μ-H**1**$^{\mathbf{NH}}$]$^+$ under conditions where [*t*-H**1**$^{\mathbf{NH}}$]$^+$ is undetectable. A sequence of three processes is invoked to explain the formation the μ-hydride under these conditions: (i) *N*-protonation, albeit unfavorable, (ii) tautomerization of ammonium species to the terminal hydride [*t*-H**1**$^{\mathbf{NH}}$]$^+$, and (iii) isomerization of [*t*-H**1**$^{\mathbf{NH}}$]$^+$ to [μ-H**1**$^{\mathbf{NH}}$]$^+$. The pK_a of [*t*-H**1**$^{\mathbf{NH}}$]$^+$ is estimated at 16, and the pK_a of [μ-H**1**$^{\mathbf{NH}}$]$^+$ is > 18.6 (MeCN scale). Being a stronger acid, [*t*-H**1**$^{\mathbf{NH}}$]$^+$ is more easily reduced than is [μ-H**1**$^{\mathbf{NH}}$]$^+$.

For both the pdt and adt derivatives, the terminal hydrides reduce at potentials that are 100 – 200 mV more positive than the corresponding bridging hydrides. The difference in reduction potentials between the isomeric hydrides is proposed to reflect differences in the localization of the reduction. In the case of the μ-hydride isomer, reduction is likely more delocalized between the two equivalent Fe atoms.[38] When the hydride is bound to a single Fe atom, reduction likely occurs at the non-hydride containing Fe atom.[39] The crystallographic results presented above indicate how this reduction could induce the formation of a mixed valence dihydrogen complex (eq 1). This scenario underscores the role of electron transfer, perhaps PCET,[40] in HER. Upon reduction, hydrogen evolution would produce the mixed valence derivative, analogous to the H_{ox} state of the enzyme (Scheme 3).

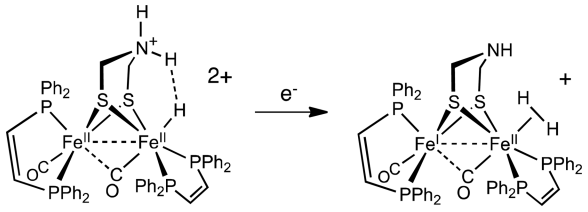

(1)

In HER catalyzed by [μ-H**1**$^{\mathbf{NH}}$]$^+$, it is apparent that **1**$^{\mathbf{NH}}$ is not regenerated. Otherwise, we would have observed increased rates during the electrolysis since [*t*-H**1**$^{\mathbf{NH}}$]$^+$ is such an active catalyst. We conclude therefore that the μ-hydride ligand in [μ-H**1**$^{\mathbf{NH}}$]$^+$ is a spectator. A related mechanism was invoked by Talarmin for catalysis by [Fe_2(pdt)(μ-H)$(CO)_4$(dppe)]$^+$.[41]

Although the bio-inspired complexes described in this report are highly active proton reduction catalysts,[42] challenges remain. These biomimetic catalysts suffer from relatively negative reduction potentials leading to high overpotentials.[1] One possible solution involves

incorporation of redox-active center to mediate the proton-coupled electron transfer that is implicated for the breaking and making of the H-H bond.[40]

Experimental

Reactions were typically conducted using Schlenk techniques at room temperature. Most reagents were purchased from Aldrich and Strem. Solvents were HPLC-grade and dried by filtration through activated alumina or distilled under nitrogen over an appropriate drying agent. $HBF_4{\cdot}Et_2O$ (Sigma-Aldrich) was supplied as 51–57% HBF_4 in Et_2O (6.91 – 7.71 M). $[H(OEt_2)_2]BAr^F{}_4$ was prepared by literature methods.[43] $[Bu_4N]PF_6$ was purchased from GFS Chemicals and was recrystallized multiple times by extraction into acetone followed by precipitation by ethanol. ^1H NMR spectra (500 and 400 MHz) are referenced to residual solvent referenced to TMS. $^{31}P\{^1H\}$ NMR spectra (202 or 161 MHz) were referenced to external 85% H_3PO_4. FT-IR spectra were recorded on a Perkin Elmer Spectrum 100 FT-IR spectrometer. CF_3CO_2D was purchased from Sigma-Aldrich. CCl_2HCO_2D was prepared by treating the acid in D_2O,

$Fe_2(adt^{NH})(CO)_4(dppv)$

A solution of $Fe_2(adt^{NH})(CO)_6$[44] (175 mg, 0.45 mmol) and dppv (179 mg, 0.45 mmol) in 15 mL of toluene was treated with a solution of anhydrous Me_3NO (34 mg, 0.45 mmol) in ca. 5 mL of MeCN. Bubbles appeared, and the reaction mixture darkened. After heating the mixture at reflux for 5 h, the FT-IR spectrum indicated complete conversion to product. Solvent was removed under vacuum, and the product was extracted into 5 mL of CH_2Cl_2. Addition of 50 mL of hexane precipitated the product. Yield: 0.260 g (80%). FT-IR, ^1H NMR, and ^{31}P NMR results matched reported values.[24]

$Fe_2(adt^{NH})(CO)_2(dppv)_2$, ($\mathbf{1^{NH}}$)

A solution of $Fe_2(adt^{NH})(CO)_4(dppv)$ (400 mg, 0.55 mmol) in 40 mL of toluene was treated with dppv (872 mg, 2.2 mmol) in 10 mL of toluene. The mixture was irradiated at 365 nm until the conversion was complete (~24 h) as indicated by IR spectroscopy. The solvent was removed in vacuum, and the product was extracted into ~3 mL of toluene. The green product precipitated upon addition of methanol to the toluene extract. The product was then re-extracted into ~2 mL of CH_2Cl_2, and the product precipitated as an olive-green powder upon the addition of 100 mL of hexanes. Yield: 150 mg (26%). ^1H NMR (500 MHz, CD_2Cl_2): δ 8.1 – 7.0 (m, 40H, $P(C_6\mathit{H_5})_2$), 2.3 (s, 4H, $(SC\mathit{H_2})_2NH$). ^{31}P NMR (CD_2Cl_2, 20 °C): δ 92. ^{31}P NMR (CD_2Cl_2, −70 °C): δ 102.6, 93.4, 92.2, 88.6. FT-IR (CH_2Cl_2): ν_{CO} = 1888, 1868 cm^{-1}. Anal. Calcd for $C_{56}H_{49}Fe_2O_2NP_4S_2{\cdot}CH_2Cl_2{\cdot}CH_3OH$ (found): C, 58.8 (58.15); H, 4.68 (4.63), N 1.18 (1.10). Diffraction quality crystals were grown at −20 °C from a CH_2Cl_2 solution of **1** layered with pentane.

$[HFe_2(adt^{NH})(CO)_2(dppv)_2]BAr^F{}_4$, ($[\mathit{t}\text{-}H\mathbf{1^{NH}}]BAr^F{}_4$), $[Fe_2(adt^{NH})(CO)_2(dppv)_2]BAr^F{}_4$ ($[\mu\text{-}H\mathbf{1^{NH}}]BAr^F{}_4$), and $[Fe_2(adt^{NH2})(\mu\text{-}H)(CO)_2(dppv)_2](BAr^F{}_4)_2$ ($[\mu\text{-}H\mathbf{1^{NH2}}](BAr^F{}_4)_2$)

In a J. Young NMR tube, ~ 0.5 mL of CD_2Cl_2 was distilled and frozen onto $\mathbf{1^{NH}}$ (5 mg, 0.005 mmol) and $[H(OEt_2)_2]BAr^F{}_4$ (5 mg, 0.005 mmol) in a −78 °C bath. The sample was then thawed and analyzed by NMR spectroscopy. ^1H NMR (600 MHz, CD_2Cl_2, −80 °C): δ −4.2 (t, Fe-H, $^2J_{PH}$ = 73 Hz). $^{31}P\{^1H\}$ NMR (242 MHz, CD_2Cl_2, −40 °C): δ 103.2 (s), 94.5 (s), 84.0 (s), 75.1 (s). Selective ^{31}P decoupling of the ^1H NMR verified that only the signals at δ 94 and 84 were coupled to the hydride, presumably these correspond to dibasal phosphines attached to the FeH center. At the sample temperature of −10 °C, a triplet of triplets at δ −14.8 (Fe-μH, J_{PH} = 25, 5 Hz) appears in the ^1H NMR spectrum, and singlets at δ 91.0 and 90.8 appear in the ^{31}P NMR spectrum, which are assigned to *sym*-$[\mu\text{-}H\mathbf{1^{NH}}]BAr^F{}_4$. Upon warming the sample to 20 °C, signals corresponding to $[\mathit{t}\text{-}H\mathbf{1^{NH}}]BAr^F{}_4$

disappear, and only *sym*-[μ-H**1**^{NH}]BAr^F_4 is observed. After ~10 min. at 20 °C, an additional ^{1}H NMR multiplet at δ-13.7 appears, and four ^{31}P NMR singlets appear at δ 88.2, 85.7, 82.7, and 77.3, which are assigned to *unsym*-[μ-H**1**^{NH}]BAr^F_4. After ~12 h at room temperature, the ratio of the *sym:unsym* isomers is 1:5.

Upon addition of a second equiv of $[H(OEt_2)_2]BAr^F_4$ (5 mg, 0.005 mmol) to the solution, the ^{1}H NMR spectrum showed a triplet of triplets at δ −15.5 (Fe-μH, J_{PH} = 25, 5 Hz) assigned to *sym*-[μ-H**1**^{NH2}]$(BAr^F_4)_2$ and a multiplet at δ −14.3 assigned to *unsym*-[μ-H**1**^{NH2}]$(BAr^F_4)_2$. Additionally, in the ^{31}P NMR spectrum signals are observed at 91.3 and 88.7 (*sym*-[μ-H**1**^{NH2}]$(BAr^F_4)_2$) and at δ 92.3, 86.0, 82.4, and 79.0 (*unsym*-[μ-H**1**^{NH2}]$(BAr^F_4)_2$). The two isomers are present in a ratio of 5:1 *sym*:*unsym*. An IR spectrum of the CD_2Cl_2 solution features bands at 1967 and 1985 cm^{-1}.

[*t*-HFe$_2$(adt^{NH2})(CO)$_2$(dppv)$_2$](BAr$^F_4$)$_2$, [*t*-H1^{NH2}] (BAr$^F_4$)$_2$

In a J. Young NMR tube, ~ 0.5 mL of CD_2Cl_2 was distilled onto **1**^{NH} (5 mg, 0.005 mmol) and $[H(OEt_2)_2]BAr^F_4$ (10 mg, 0.010 mmol). The J. Young tube was then gently warmed to near −78 °C before analysis by low temperature NMR spectroscopy. High field ^{1}H NMR (600 MHz, CD_2Cl_2, −40 °C): δ - 4.95 (t, Fe-H, $^2J_{PH}$ = 72 Hz). ^{31}P{^{1}H} NMR (242 MHz, CD_2Cl_2, −40 °C): δ 98 (s), 89 (s), 76 (s), 74 (s). Decoupling experiments verified that the high field ^{1}H NMR signal is coupled to the ^{31}P NMR signals at δ 89 and 74.

Crystallization of [*t*-HFe$_2$(adt^{NH2})(CO)$_2$(dppv)$_2$]BF$_4$)$_2$

Crystals were obtained by treating a CH_2Cl_2 solution of **1**^{NH}, at 0 °C, with two equiv of $HBF_4{\cdot}Et_2O$ and layering with cold pentane. Storage at −20 °C gave dark brown crystals.

[Fe$_2$(adt^{NH})(μ-H)(CO)$_2$(dppv)$_2$]BAr$^F_4$, [μ-H1^{NH}]BAr$^F_4$

A 10 mL solution of **1**^{NH} (35 mg, 0.03 mmol) in CH_2Cl_2 was treated with a 5-mL solution of $[H(OEt_2)_2]BAr^F_4$ (33 mg, 0.03 mmol) in CH_2Cl_2. Within 5 min., the solution color changed from green to brown. After stirring at room temperature for 22 h, the solution was concentrated to ~ 5 mL, and the brown product was precipitated with addition of 20 mL of Et_2O. IR (CH_2Cl_2): ν_{CO} = 1948, 1969 (sh) cm^{-1}. ^{1}H and ^{31}P NMR data match those described above. Anal. Calcd for $C_9H_{62}BF_{24}Fe_2NO_2P_4S_2{\cdot}2CH_2Cl_2{\cdot}C_4H_{10}O$ (found): C, 51.89 (52.19); H, 3.52 (3.13); N 0.64 (0.76).

Protonation of Fe$_2$(adt^{NH})(CO)$_2$(dppv)$_2$ with 1.5 equiv of [H(OEt$_2$)$_2$] BAr$^F_4$

In a J. Young NMR tube CD_2Cl_2 was distilled onto **1**^{NH} (5 mg, 0.005 mmol) and $[H(OEt_2)_2]BAr^F_4$ (7.5 mg, 0.0075 mmol). The J. Young tube was then gently warmed to near −78 °C before analysis by low temperature NMR spectroscopy. High field ^{1}H NMR (600 MHz, CD_2Cl_2, −40 °C): δ - 4.95 (Fe-*H*, $^2J_{PH}$ = 72 Hz), −4.2 (Fe-H, $^2J_{PH}$ = 73 Hz).

Effect of [Bu$_4$N]BF$_4$ on Equilibrium between Tautomers [*t*-H1^{NH}]$^+$ and [1^{NH2}]$^+$

A 7 mM solution of [*t*-H**1**^{NH}]BAr^F_4 was prepared by dissolving **1**^{NH} (15 mg, 0.014 mmol) and $[H(Et_2O)_2]BAr^F_4$ (15 mg, 0.014 mmol) in 2 mL of CH_2Cl_2, which had been pre-cooled to −78 °C. Aliquots of a 0.6 M $[Bu_4N]BF_4$ solution were added to the solution. After each addition, 0.1 mL aliquots were removed and immediately analyzed by IR spectroscopy.

[*t*-HFe$_2$(pdt)(μ-CO)(CO)(dppv)$_2$]BF$_4$, [*t*-H2]BF$_4$

A dark green solution of **2** (205 mg, 0.192 mmol) in 5 mL of CH_2Cl_2 was treated at −40 °C with $HBF_4{\cdot}Et_2O$ (5 mL 0.04 M, 0.2 mmol). The resulting darker green solution was then diluted with 100 mL of cold (−78 °C) Et_2O, producing a green precipitate. The precipitate

was collected by filtration at −78 °C, washed with 2×10 mL of Et_2O, and dried under vacuum, prior to storage at −30 °C. Yield: 140 mg (63%). ^{1}H NMR (500 MHz, CD_2Cl_2): δ −3.5 (t, Fe-H, $^2J_{PH}$ = 76 Hz). $^{31}P\{^1H\}$ NMR (202 MHz, CD_2Cl_2): δ 99 (s), 91 (s), 86 (s), 68 (s). Selective ^{31}P decoupled ^{1}H NMR verified that the signals at δ 91 and 86 coupled to the hydride signal. FT-IR (CH_2Cl_2, cm^{-1}): ν_{CO} = 1965, 1905, 1988.

$[Fe_2(pdt)(\mu\text{-}H)(CO)_2(dppv)_2]PF_6$, [μ-H2]$PF_6$

In a 250-mL Schlenk flask, a dark green solution of **1** (200 mg, 0.187 mmol) in 5 mL of CH_2Cl_2 was treated at room temperature with a solution of 2.0 M HCl in Et_2O (0.2 mL, 0.2 mmol). Solvent was removed under vacuum, and the solid was redissolved in MeOH. The product was precipitated as its PF_6^- salt by addition of ca. 5 mL of a saturated aqueous solution of NH_4PF_6. The brownish precipitate was then transferred anaerobically onto a Celite plug in a chromatography column where it was washed with 6 × 30 mL of H_2O and 6 × 30 mL of Et_2O. The product was then extracted off the Celite with CH_2Cl_2, and solvent removed under vacuum. The product was dissolved with 5 mL of CH_2Cl_2, which was diluted with 5 mL of MeOH. Addition of 50 mL of hexane to this solution yielded a brown powder, which was collected by filtration and dried. Yield: 170 mg (75%). High-Field ^{1}H NMR (500 MHz, CD_2Cl_2): δ - 14.5 (dddd, μ-H, J_{PH1} = 24, J_{PH2} = 19, J_{PH3} = 10 Hz), −15.6 (tt, μ-H, J_{PH1} = 24, J_{PH2} = 6 Hz). $^{31}P\{^1H\}$ NMR (202 MHz, CD_2Cl_2): δ 89.6 (s), 89.6 (s), δ 76.7 (s), 82.8 (s), 84.2 (s), 87.8 (s). FT-IR (CH_2Cl_2, cm^{-1}): ν_{CO} = 1963, 1951. Anal. Calcd for $C_{57}H_{51}F_6Fe_2O_2P_5S_2$ (found): C, 56.45 (56.28); H, 4.24 (4.28); Fe 9.21 (8.79).

Electrochemistry

Electrochemical experiments were carried out on CH Instruments Model 600D Series Electrochemical Analyzer or a BAS-100 Electrochemical Analyzer. Cyclic voltammetry experiments were conducted using a 10-mL one-compartment glass cell with a tight-fitting Teflon top. The working electrode was a glassy carbon (GC) disk (diameter = 3.00 mm). A silver wire was used as a quasi-reference electrode, and the counter electrode was a Pt wire. Ferrocene was added as an internal reference, and each cyclic voltammogram was referenced to this $Fc^{0/+}$ couple = 0.00 V. *i*R compensation was applied to all measurements using the CH Instruments or BAS software. Cell resistance was determined prior to each scan, and the correction applied to the subsequently collected cyclic voltammogram. During prolonged experiments, additional solvent was added to compensate for evaporative loss. Between scans, the solution was purged briefly with N_2 and the working GC electrode was removed and polished. The duration of typical electrochemical titrations was 30 min. For all experiments, the electrolyte solution was prepared and sparged in the cell, which was fitted with electrodes. A CV of the electrolyte was collected prior to the addition of Fe_2 compound, in order to check the purity of the electrolyte. The diiron compound was then dissolved in the electrolyte solution and transferred to the cell.

Due to their tendency to isomerize above 0 °C, [*t*-H$\mathbf{1}^{\mathbf{NH}}$]$^+$, [*t*-H$\mathbf{1}^{\mathbf{NH2}}$]$^{2+}$, and [*t*-H**2**]$^+$ were generated *in-situ*. The corresponding bridging hydrides were isolated as their BF_4^- salts prior to electrochemical experiments. All electrochemical experiments were conducted at 0 °C.

Supplementary Material

Refer to Web version on PubMed Central for supplementary material.

Acknowledgments

This work was supported by the National Institutes of Health (Grant GM61153). This work was also supported in part by the ANSER Center, an Energy Frontier Research Center funded by the U.S. Department of Energy, Office

of Science, Office of Basic Energy Sciences, under Award Number DE-SC0001059. We thank Danielle Gray for collecting crystallographic data.

REFERENCES

1. Fontecilla-Camps JC, Volbeda A, Cavazza C, Nicolet Y. Chem. Rev. 2007; 107:4273. [PubMed: 17850165]
2. Cammack, R.; Frey, M.; Robson, R. Hydrogen as a Fuel: Learning from Nature. London: Taylor & Francis; 2001.
3. Fontecilla-Camps JC, Amara P, Cavazza C, Nicolet Y, Volbeda A. Nature. 2009; 460:814. [PubMed: 19675641]
4. Tard C, Pickett CJ. Chem. Rev. 2009; 109:2245. [PubMed: 19438209]
5. Rakowski DuBois M, DuBois DL. Acc. Chem. Res. 2009; 42:1974. [PubMed: 19645445] Bullock, RM., editor. Catalysis without Precious Metals. Wiley-VCH; Weinheim: 2010.
6. Peters JW, Lanzilotta WN, Lemon BJ, Seefeldt LC. Science. 1998; 282:1853. [PubMed: 9836629]
7. Frey M. ChemBioChem. 2002; 3:153. [PubMed: 11921392]
8. Silakov A, Wenk B, Reijerse E, Lubitz W. Phys. Chem. Chem. Phys. 2009; 11:6592. [PubMed: 19639134]
9. Tschierlei S, Ott S, Lomoth R. Ener. & Envir. Sci. 2011; 4:2340.
10. Nametkin NS, Tyurin VD, Kukina MA. Russ. Chem. Rev. 1986; 55:439.Linford L, Raubenheimer HG. Adv. Organometal. Chem. 1991; Volume 32:1.
11. Schmidt M, Contakes SM, Rauchfuss TB. J. Am. Chem. Soc. 1999; 121:9736.Le Cloirec A, Davies SC, Evans DJ, Hughes DL, Pickett CJ, Best SP, Borg S. Chem Commun. 1999; 2285Lyon EJ, Georgakaki IP, Reibenspies JH, Darensbourg MY. Angew. Chem. Int. Ed. 1999; 38:3178.Gloaguen F, Lawrence JD, Schmidt M, Wilson SR, Rauchfuss TB. J. Am. Chem. Soc. 2001; 123:12518. [PubMed: 11741415]
12. Gloaguen F, Rauchfuss TB. Chem. Soc. Rev. 2009; 38:100. [PubMed: 19088969]
13. Barton BE, Olsen MT, Rauchfuss TB. J. Am. Chem. Soc. 2008; 130:16834. [PubMed: 19053433]
14. Nakazawa H, Itazaki M. Top. Organomet. Chem. 2011; 33:27.
15. Matthews SL, Heinekey DM. Inorg. Chem. 2010; 49:9746. [PubMed: 20883039]
16. Bruschi M, Greco C, Kaukonen M, Fantucci P, Ryde U, De Gioia L. Angew. Chem. Int. Ed. 2009; 48:3503.
17. Ezzaher S, Capon JF, Gloaguen F, Petillon FY, Schollhammer P, Talarmin J, Pichon R, Kervarec N. Inorg. Chem. 2007; 46:3426. [PubMed: 17397148]
18. Barton BE, Zampella G, Justice AK, De Gioia L, Rauchfuss TB, Wilson SR. Dalton Trans. 2010; 39:3011. [PubMed: 20221534]
19. Barton BE, Rauchfuss TB. Inorg. Chem. 2008; 47:2261. [PubMed: 18333613]
20. van der Vlugt JI, Rauchfuss TB, Whaley CM, Wilson SR. J. Am. Chem. Soc. 2005; 127:16012. [PubMed: 16287273]
21. Singleton ML, Jenkins RM, Klemashevich CL, Darensbourg MY. C. R. Chim. 2008; 11:861.
22. Winter A, Zsolnai L, Huttner G. Z. Naturforsch. 1982; 37b:1430.
23. Lambert JB, Featherman SI. Chem. Rev. 1975; 75:611.
24. Justice AK, Zampella G, De Gioia L, Rauchfuss TB, van der Vlugt JI, Wilson SR. Inorg. Chem. 2007; 46:1655. [PubMed: 17279743]
25. Ott S, Kritikos M, Akermark B, Sun L, Lomoth R. Angew. Chem. Int. Ed. 2004; 43:1006.Schwartz L, Eilers G, Eriksson L, Gogoll A, Lomoth R, Ott S. Chem. Commun. 2006:520.
26. Lawrence JD, Li H, Rauchfuss TB, Benard M, Rohmer MM. Angew Chem. Int. Ed. 2001; 40:1768.
27. Basallote MG, Besora M, Castillo CE, Fernández-Trujillo MJ, Lledós A, Maseras F, Máñez MA. J. Am. Chem. Soc. 2007; 129:6608. [PubMed: 17465549]
28. Das P, Capon JF, Gloaguen F, Pétillon FY, Schollhammer P, Talarmin J, Muir KW. Inorg. Chem. 2004; 43:8203. [PubMed: 15606156]

29. Olsen MT, Bruschi M, De Gioia L, Rauchfuss TB, Wilson SR. J. Am. Chem. Soc. 2008; 130:12021. [PubMed: 18700771]
30. Ho NN, Bau R, Mason SA. J. Organometal. Chem. 2003; 676:85.
31. Custelcean R, Jackson JE. Chem. Rev. 2001; 101:1963. [PubMed: 11710237]
32. Izutsu, K. Acid-Base Dissociation Constants in Dipolar Aprotic Solvents. Oxford, U.K.: Blackwell Scientific Publications; 1990.
33. Felton GAN, Mebi CA, Petro BJ, Vannucci AK, Evans DH, Glass RS, Lichtenberger DL. J. Organomet. Chem. 2009; 694:2681.
34. Justice AK, De Gioia L, Nilges MJ, Rauchfuss TB, Wilson SR, Zampella G. Inorg. Chem. 2008; 47:7405. [PubMed: 18620387]
35. Felton GAN, Glass RS, Lichtenberger DL, Evans DH. Inorg. Chem. 2006; 45:9181. [PubMed: 17083215]
36. Miller, MA.; Carey, AA. Ullmann's Encyclopedia of Industrial Chemistry. Wiley-VCH; Weinheim: 2000.
37. Fourmond V, Jacques PA, Fontecave M, Artero V. Inorg. Chem. 2010; 49:10338. [PubMed: 20964310]
38. Jablonskya A, Wright JA, Fairhurst SA, Peck JNT, Ibrahim SK, Oganesyan VS, Pickett CJ. J. Am. Chem. Soc. 2011; 133:18606. [PubMed: 22035325]
39. Lever ABP. Inorg. Chem. 1990; 29:1271.
40. Camara JM, Rauchfuss TB. J. Am. Chem. Soc. 2011; 133:8098. [PubMed: 21548619] Camara JM, Rauchfuss TB. Nature Chem. 2012; 4:26. [PubMed: 22169868]
41. Ezzaher S, Capon JF, Dumontet N, Gloaguen F, Petillon FY, Schollhammer P, Talarmin J. J. Electroanal. Chem. 2009; 626:161.
42. Helm ML, Stewart MP, Bullock RM, Rakowski DuBois M, DuBois DL. Science. 2011; 333:863. [PubMed: 21836012] Cheah MH, Tard C, Borg SJ, Liu X, Ibrahim SK, Pickett CJ, Best SP. J. Am. Chem. Soc. 2007; 129:11085. [PubMed: 17705475]
43. Brookhart M, Grant B, Volpe AF. Organometallics. 1992; 11:3920.
44. Zaffaroni R, Rauchfuss TB, Gray DL, De Gioia L, Zampella G. to be submitted.

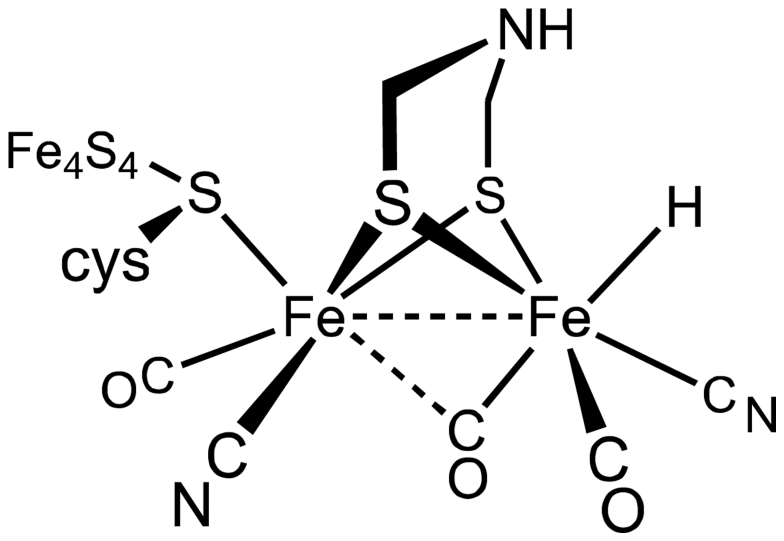

Figure 1.
Structure proposed for the active site of [FeFe]-hydrogenase in the H_{red} state.[1]

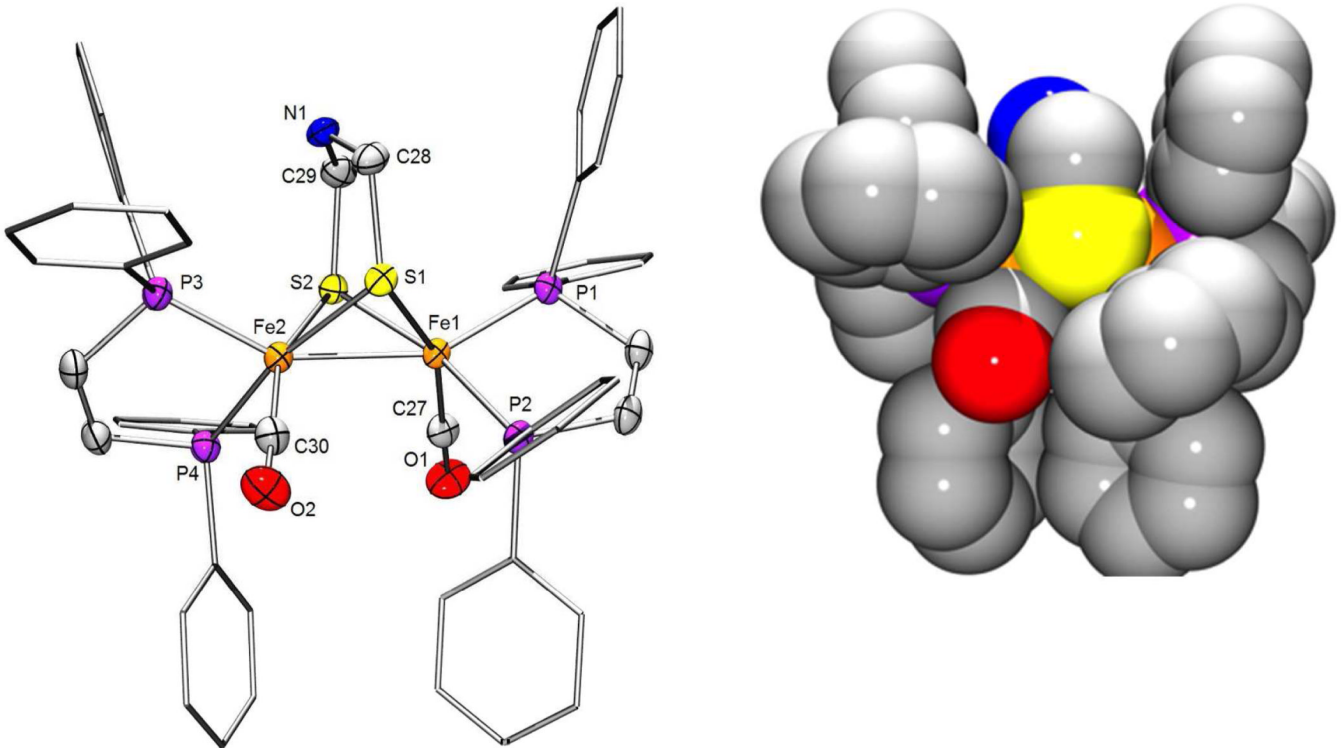

Figure 2.

Structure of $Fe_2(adr^{NH})(CO)_2(dppv)_2$ (**1**^{NH}). Left: with thermal ellipsoids drawn at the 50 % Selected distances (Å): Fe1-Fe2, 2.6027(6); Fe1-C27, 1.7381(30); Fe1-P1, 2.1884(8); Fe1-P2, 2.2108(8); Fe1-S1, 2.2108(8); Fe1-S2, 2.2668(8); Fe2-C30, 1.7508(30); Fe2-P3, 2.1937(9); Fe2-P4, 2.2296(8); Fe2-S1, 2.2785(8); Fe2-S2, 2.2668(8). Right: space-filling model showing that the Ph groups block the Fe-Fe bond (red = O, blue = N, yellow = S, orange = Fe, violet = P).

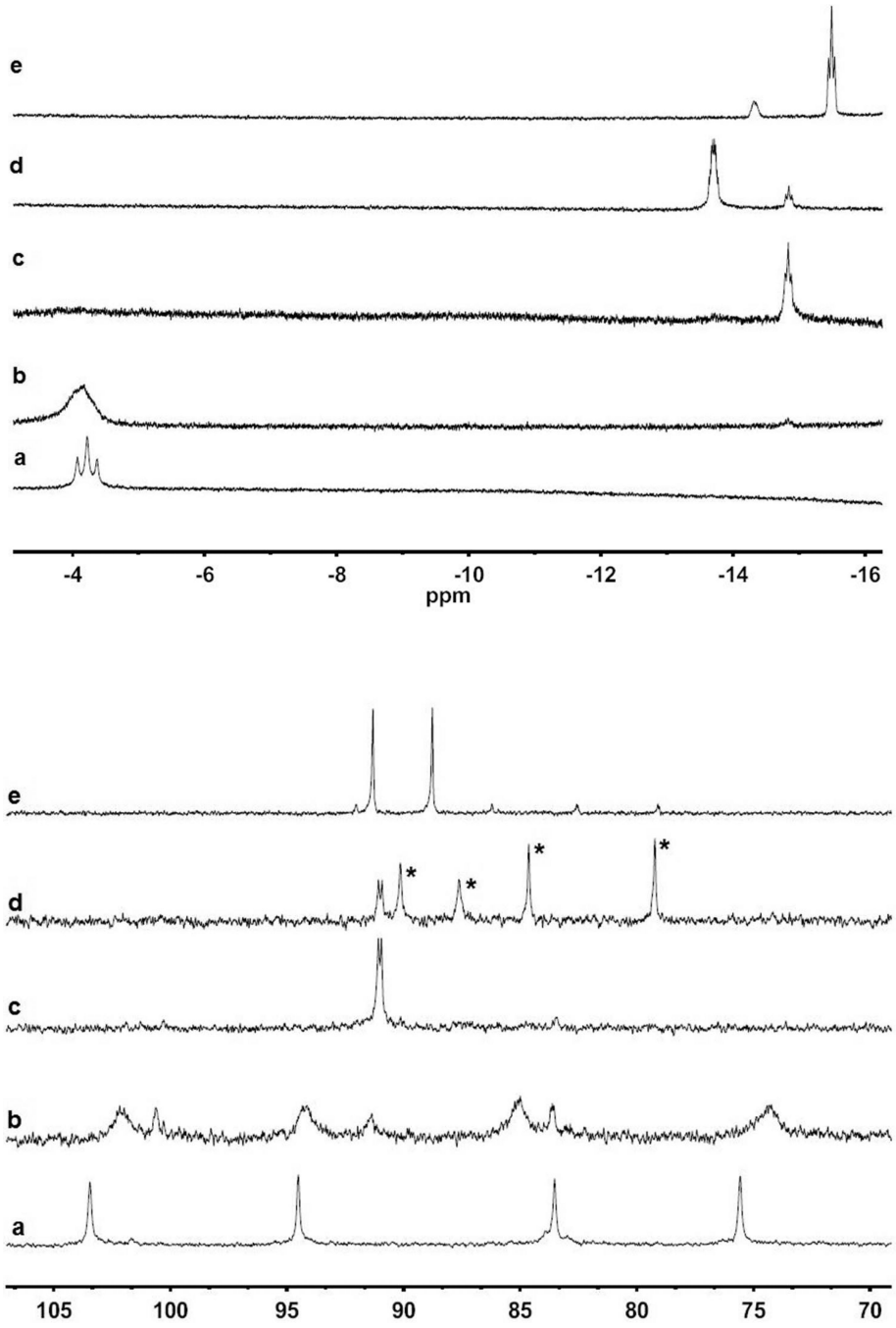

Figure 3.

^{1}H and ^{31}P NMR spectra of the protonation of **1**^{NH} with $[H(OEt_2)_2]BAr^F{}_4$ in CD_2Cl_2 at various times and temperatures. Spectra a: −80 °C ([*t*-H**1**^{NH}]$^+$). Spectra b: sample warmed to −10 °C. Spectra c: sample warmed to 20 °C (*sym*-[μ-H**1**^{NH}]$^+$, this spectrum does not change upon recooling to 0 °C). Spectra d: previous sample after standing at 20 °C for 24 h, (*sym*- and *unsym*-[μ-H**1**^{NH}]$^+$, the latter indicated by asterisks). Spectra e: same sample after addition of 1 equiv of $[H(OEt_2)_2]BAr^F{}_4$ (mainly *sym*-[μ-H**1**^{NH2}]$^{2+}$ and a small amount of the *unsym* isomer).

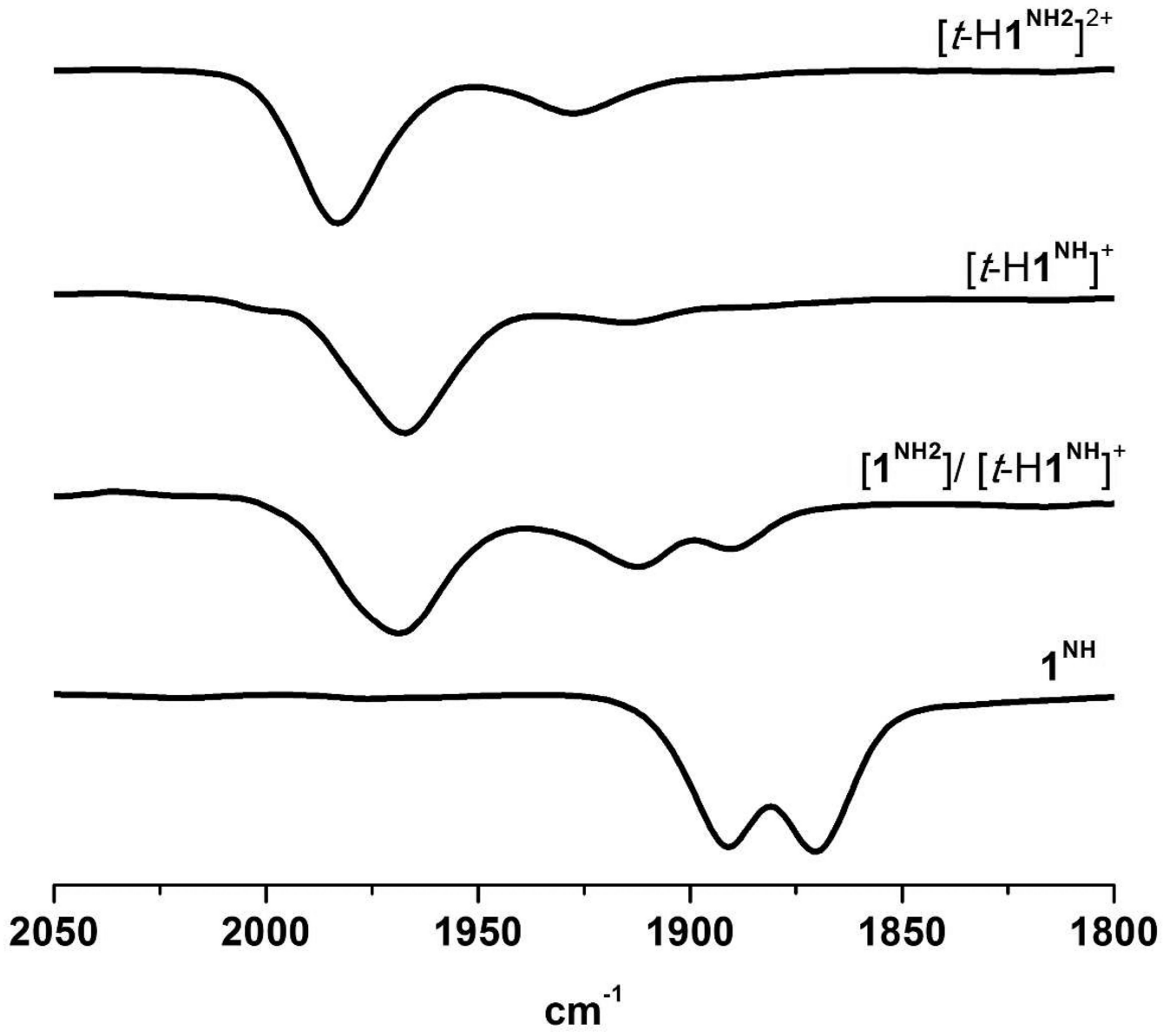

Figure 4.

FT-IR spectra in the ν_{CO} region of $\mathbf{1}^{\mathbf{NH}}$ (bottom) and products from its protonation in CH_2Cl_2. A mixture of the ammonium cation $[\mathbf{1}^{\mathbf{NH2}}]^+$ and $[t\text{-H}\mathbf{1}^{\mathbf{NH}}]^+$ generated by addition of excess $[Bu_4N]BF_4$ to a solution of $[t\text{-H}\mathbf{1}^{\mathbf{NH}}]^+$. The terminal hydride, $[t\text{-H}\mathbf{1}^{\mathbf{NH}}]^+$, formed by protonation of **1** with one equiv of $[H(OEt_2)_2]BAr^F{}_4$ at −40 °C. The terminal hydride ammonium dication $[t\text{-H}\mathbf{1}^{\mathbf{NH2}}]^{2+}$ formed by protonation of $\mathbf{1}^{\mathbf{NH}}$ with 2 equiv of HBF_4•Et_2O at −40 °C.

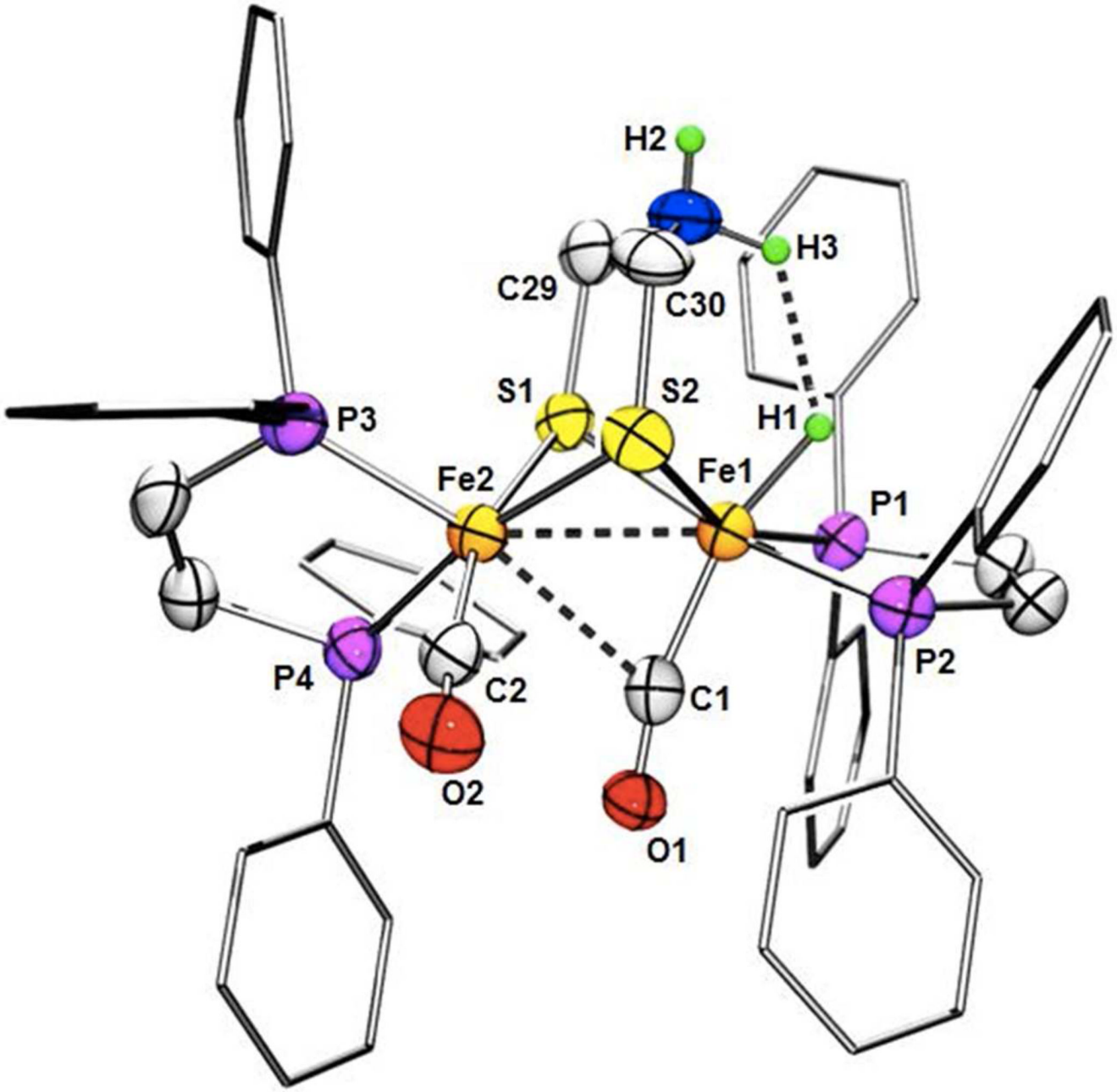

Figure 5.

Structure of [*t*-HFe$_2$(adt^{NH2})(CO)$_2$(dppv)$_2$](BF$_4$)$_2$, [*t*-H**1**^{NH2}](BF$_4$)$_2$. Counter ions and solvent of crystallization are not shown. Selected distances (Å): H1---H2, 1.88(7); Fe1-C1, 1.794(5); Fe1-P2, 2.2141(13); Fe1-P1, 2.2196(12); Fe1-S2, 2.2610(12); Fe1-S1, 2.3009(13); Fe1-Fe2, 2.6155(9); Fe1-H1, 1.44(4); Fe2-C2, 1.769(5); Fe2-P3, 2.2122(14); Fe2-S2, 2.2348(14); Fe2-S1, 2.2564(12); Fe2-P4, 2.2686(14). Angles (°): C1-Fe1-Fe2, 66.68(14); Fe2-Fe1-H1, 130.3(18); S2-Fe1-S1, 83.50(4); S2-Fe2-S1, 85.12(4); O1-C1-Fe1, 166.1(4).

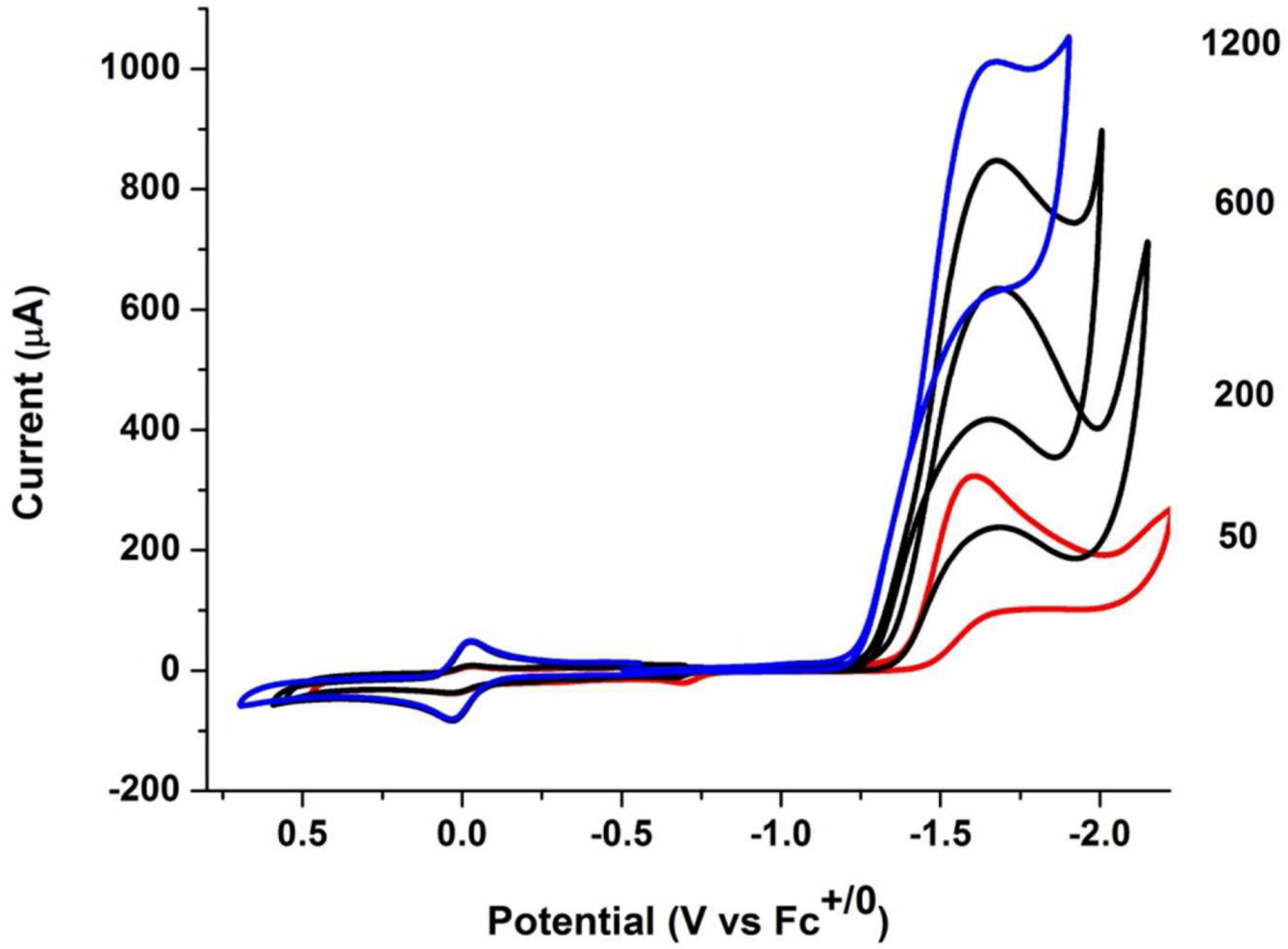

Figure 6.

Cyclic voltammograms of a 1.00 mM solution of **1**^{NH} (0 °C, 0.125 M $[Bu_4N]BAr^F{}_4$, CH_2Cl_2, scan rate = 0.5 V/s, glassy carbon working electrode, Pt counter electrode, Ag wire pseudo reference electrode, Fc internal standard) recorded with increasing equiv of $ClCH_2CO_2H$.

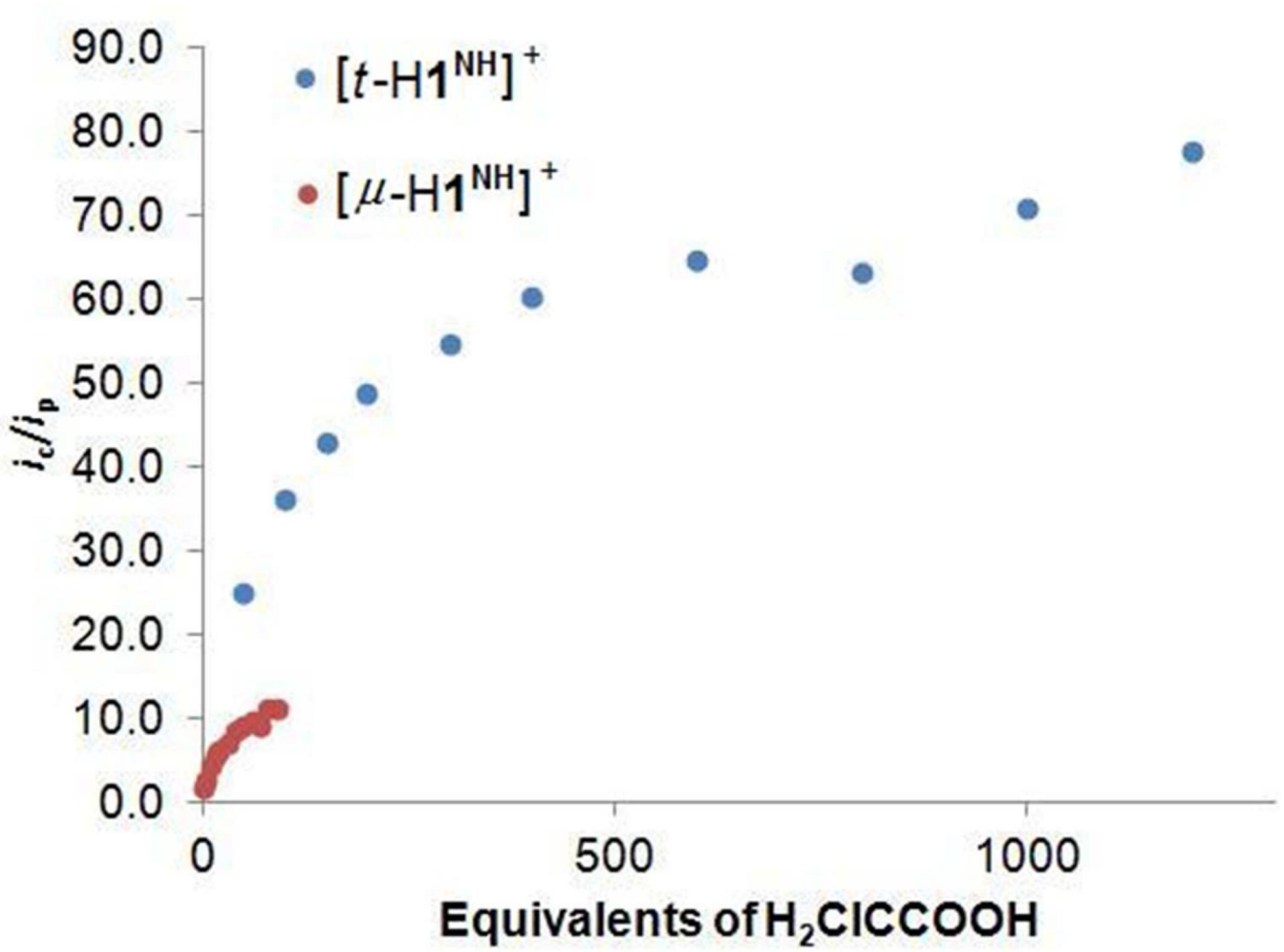

Figure 7.

Graph of i_c/i_p vs equiv acid for the addition of $ClCH_2CO_2H$ to a 1.00 mM solution of $\mathbf{1}^{\mathbf{NH}}$, with $[Bu_4N]BAr^{F4}$ as supporting electrolyte (blue) and 1.0 M solution of $[\mu\text{-H}\mathbf{1}^{\mathbf{NH}}]^+$, with $[Bu_4N]PF_6$ as supporting electrolyte (red). *Inset:* magnified data for $[\mu\text{-H}\mathbf{1}^{\mathbf{NH}}]^+$.

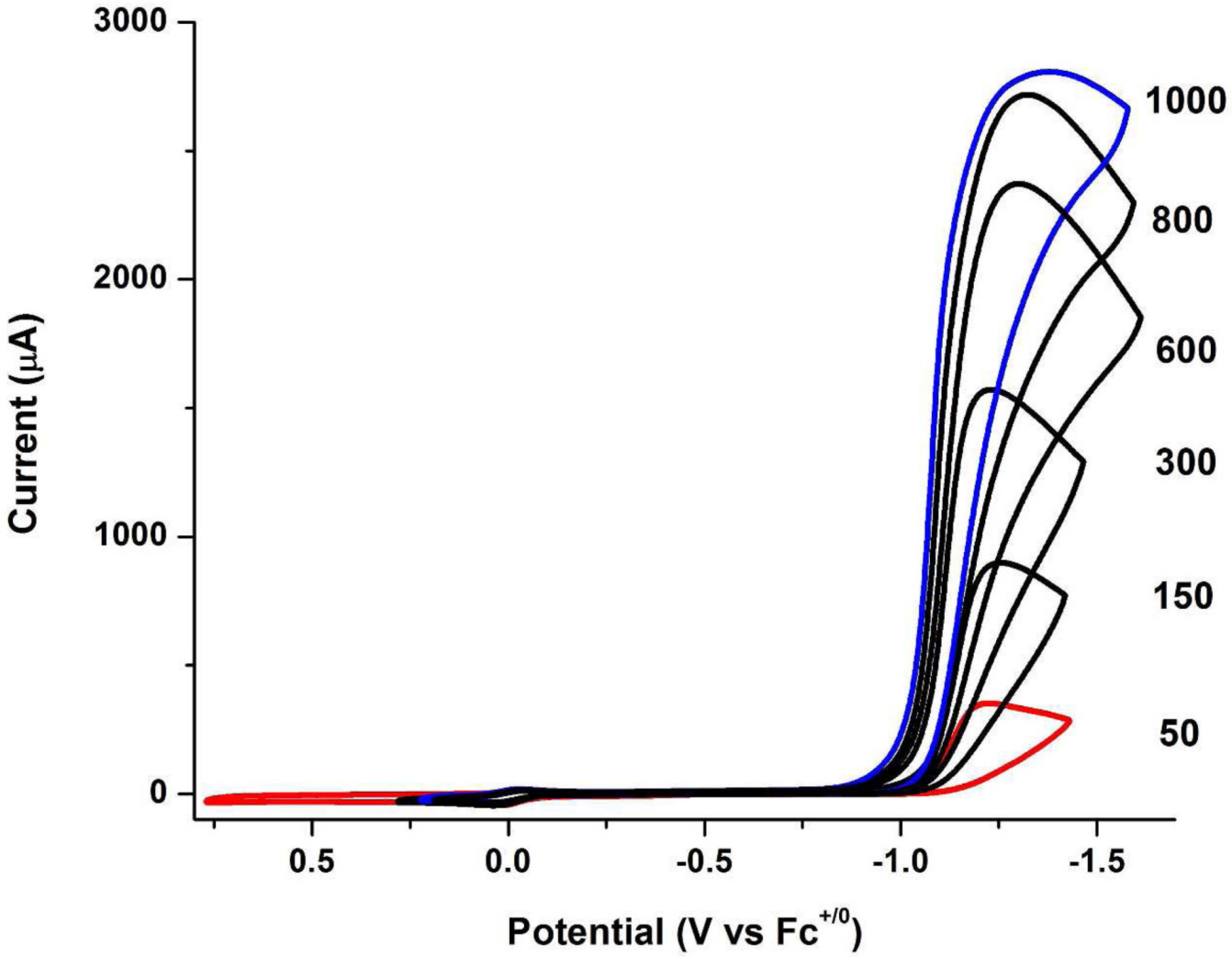

Figure 8.

Cyclic voltammograms of a 0.5 mM solution of $\mathbf{1}^{\mathbf{NH}}$ (0 °C, 0.125 M $[Bu_4N]BAr^F{}_4$, CH_2Cl_2, scan rate = 1.0 V/s, GC working electrode, Pt counter electrode, Ag wire pseudo reference electrode, Fc internal standard) recorded with increasing equiv of CF_3CO_2H.

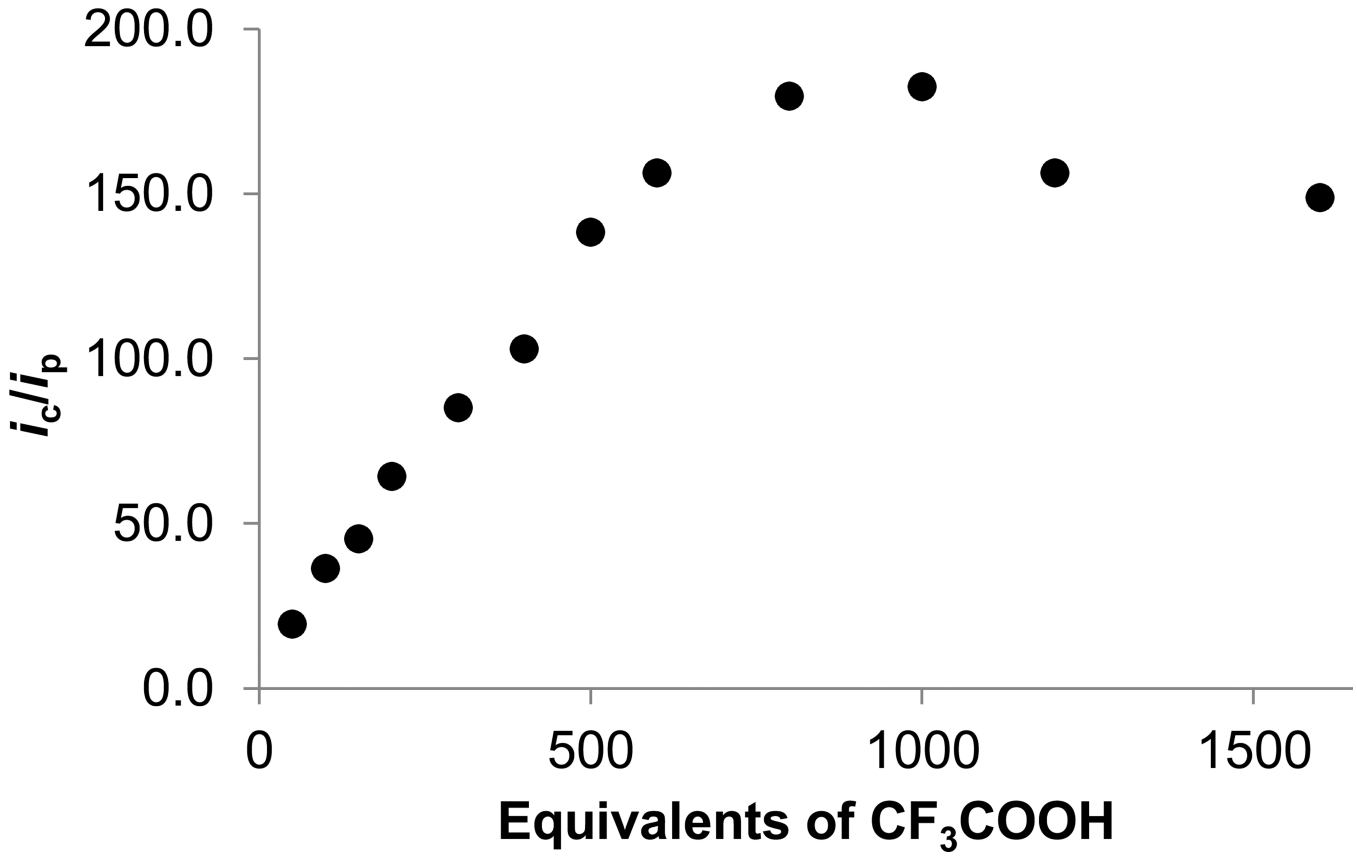

Figure 9.
Dependence of i_c/i_p on equiv of CF_3CO_2H added to a 0.5 mM solution of **1**^{NH}, with $[Bu_4N]BAr^F{}_4$ as supporting electrolyte.

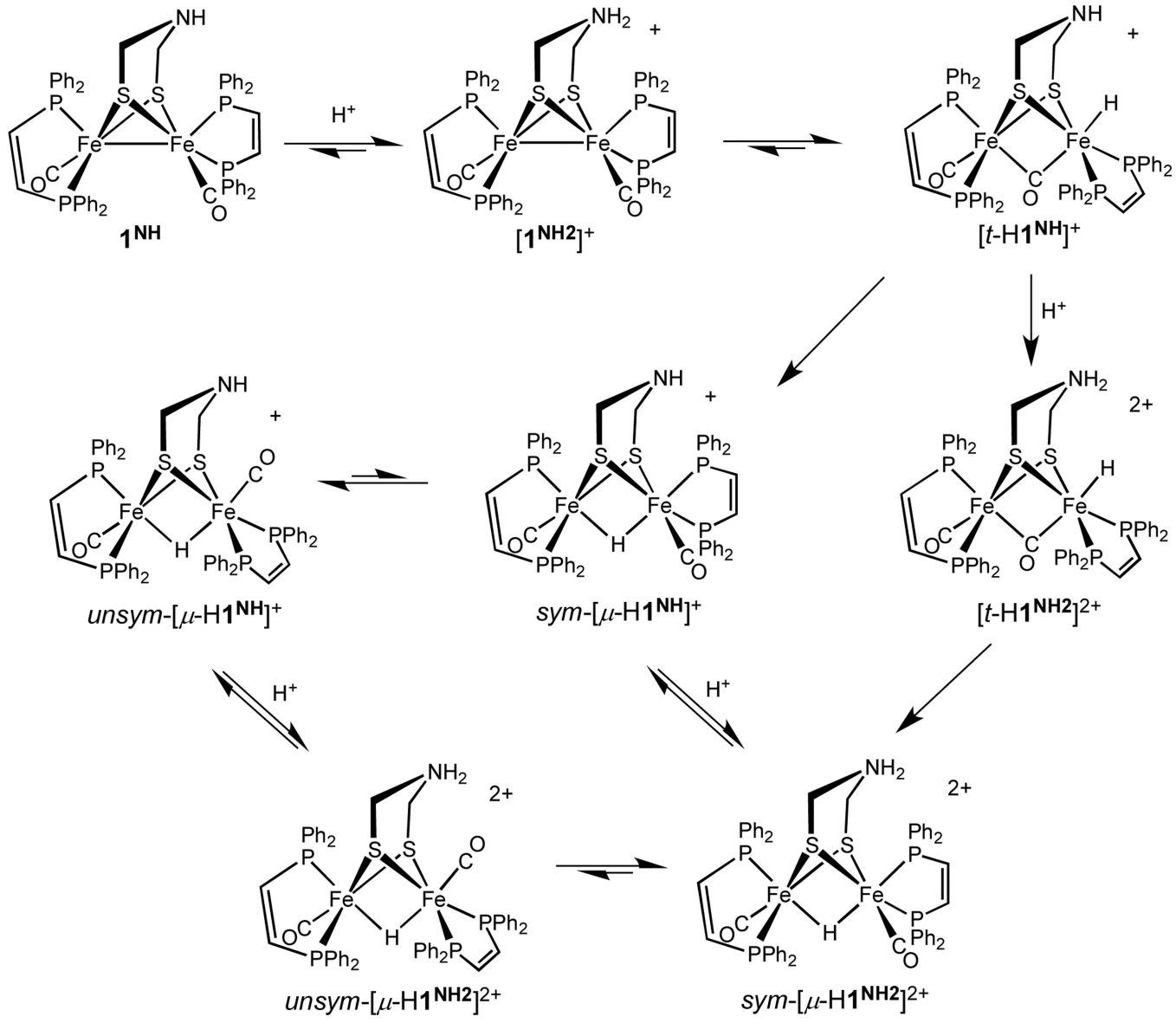

Scheme 1.
Protonation of **1**$^{\mathbf{NH}}$ and isomerization reactions of the resulting hydrides.

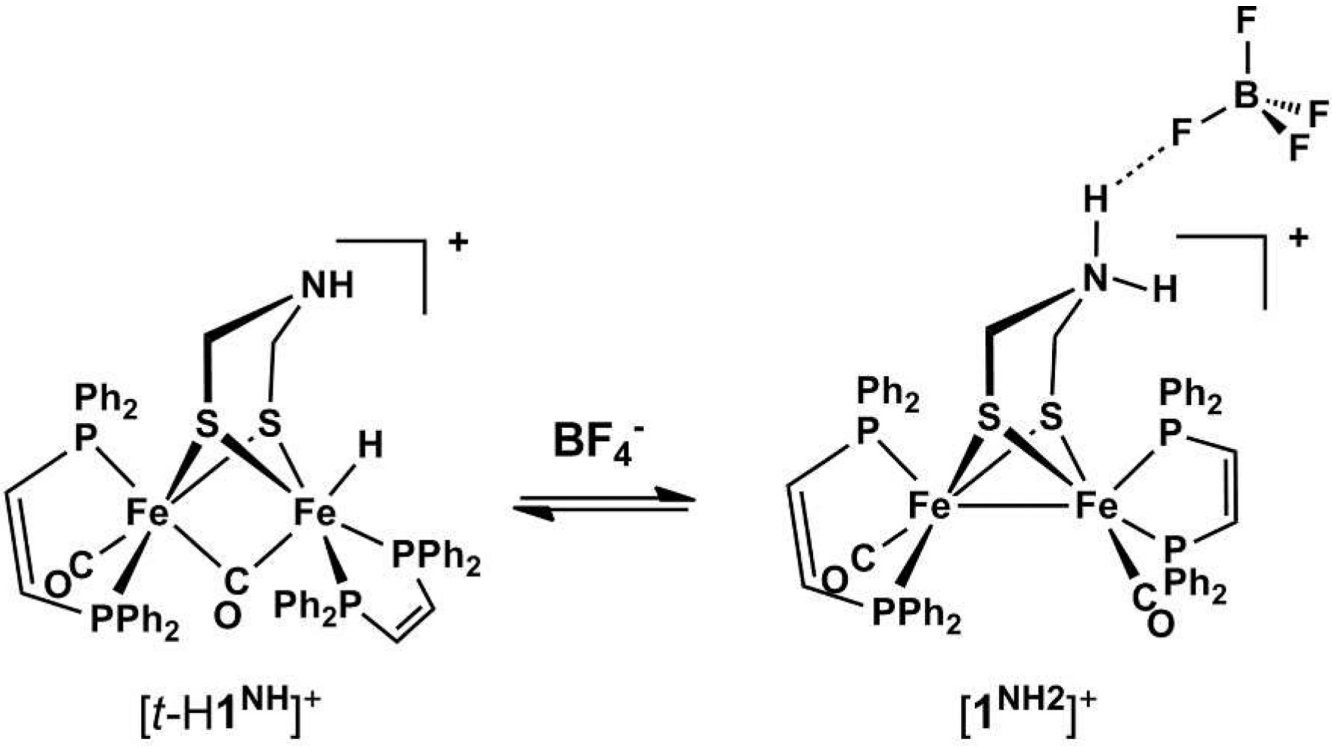

Scheme 2.
Proposed hydrogen-bonding interaction between $[\mathbf{1}^{\mathbf{NH2}}]^+$ and BF_4^- resulting in stabilization of the ammonium tautomer.

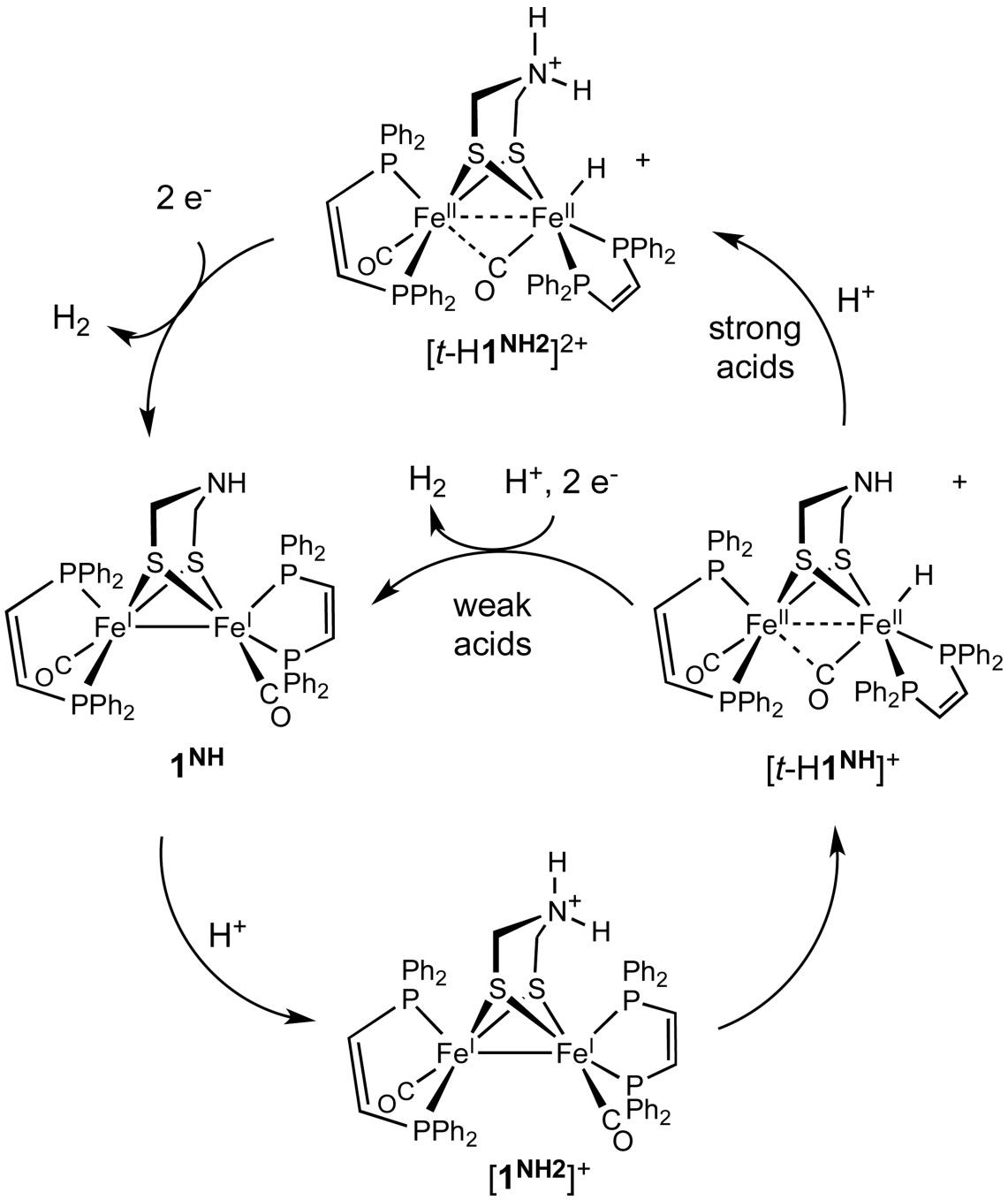

Scheme 3.
Proposed mechanism for proton reduction catalyzed by [*t*-H**1**$^{\mathbf{NH}}$]$^{+}$. Two subcycles are shown for strong and weak acids.

Table 1

Activities of [FeFe]- and [NiFe]-Hydrogenases.[1]

Reaction	FeFe	NiFe
H_2 Oxidation	28000	700
H_2 Production	6000–9000	700

Rates quoted in moles of H_2 per mole of enzyme per second measured at 30 °C.

Table 2

Spectroscopic Properties for **1^{NH}**, **2**, and Their Protonated Derivatives in CD_2Cl_2 solution.

Compound	IR: ν_{CO} (cm^{-1})	^{1}H NMR: δ Hydride (ppm)	^{31}P NMR (ppm)
$Fe_2(adt^{NH})(CO)_2(dppv)_2$, **1^{NH}**	1888, 1868	-	91.2 −70 °C: 102.6, 93.4, 92.2, 88.6
[*t*-$HFe_2(adt^{NH})(CO)_2(dppv)_2]^+$, [*t*-H**1^{NH}**]$^+$	1965, 1915	−4.2 (t) *J* = 73 Hz	103.2, 94.5, 84.0, 75.1
[*t*-$HFe_2(adt^{NH2})(CO)_2(dppv)_2]^{2+}$, [*t*-H**1^{NH2}**]$^{2+}$	1986, 1925	−4.95 (t) *J* = 72 Hz	98, 89, 76, 74
$[Fe_2(adt^{NH})(\mu\text{-H})(CO)_2(dppv)_2]^+$, *sym*-[μ-H**1^{NH}**]$^+$	not obsv'd	−14.8 (tt) *J* = 25, 5 Hz	91.1, 90.9
$[Fe_2(adt^{NH})(\mu\text{-H})(CO)_2(dppv)_2]^+$, *unsym*-[μ-H**1^{NH}**]$^+$	1948, 1969	−13.7 (dtd)	90.1, 87.6, 84.6, 79.2
$[Fe_2(adt^{NH2})(\mu\text{-H})(CO)_2(dppv)_2]^{2+}$, *sym*-[μ-H**1^{NH2}**]$^{2+}$	1967, 1985	−15.6 (tt) *J* = 20, 5 Hz	91.3, 88.7
$[Fe_2(adt^{NH2})(\mu\text{-H})(CO)_2(dppv)_2]^{2+}$, *unsym*-[μ-H**1^{NH2}**]$^{2+}$	not obsv'd	−14.5 (dtd)	92.3, 86.0, 82.4, 79.0
$Fe_2(pdt)(CO)_2(dppv)_2$, **2**	1888, 1868	-	90.8 −80 °C: 97, 88.5
$[HFe_2(pdt)(CO)_2(dppv)_2]^+$, [*t*-H**2**]$^+$	1965, 1905	−3.5 (t) *J* = 78 Hz	99, 91, 86, 68
$[Fe_2(pdt)(\mu\text{-H})(CO)_2(dppv)_2]^+$, *sym*-[μ-H**2**]$^+$	not obsv'd	−15.6 (tt) *J* = 24, 6	89.6, 89.4
$[Fe_2(pdt)(\mu\text{-H})(CO)_2(dppv)_2]^+$, *unsym*-[μ-H**2**]$^+$	1951, 1968	−14.5 (dddd) *J* = 24, 19,19, 10	76.7, 82.7, 84.2, 87.9

Table 3

Selected Electrochemical Properties of **1** and **2**, and Their Protonated Derivatives. The Electrolytes for Measurements: $[Bu_4N]BAr^F{}_4$ (for **1**) and $[Bu_4N]PF_6$ (for **2**).

Compound	$E_{1/2}$ in CH_2Cl_2 (V vs $Fc^{+/0}$)	assignment	i_{pc}/i_{pa}
[*t*-$HFe_2(adt^{\mathbf{NH}})(CO)_2(dppv)_2]^+$, [*t*-H**1**$^{\mathbf{NH}}$]$^+$	−1.64	[*t*-H**1**$^{\mathbf{NH}}$]$^{+/0}$	irreversible
[*t*-$HFe_2(adt^{NH2})(CO)_2(dppv)_2]^{2+}$, [*t*-H**1**$^{\mathbf{NH2}}$]$^{2+}$	−1.4	[*t*-H**1**$^{\mathbf{NH2}}$]$^{2+/+}$	irreversible
$[Fe_2(adt^{NH})(\mu\text{-H})(CO)_2(dppv)_2]^+$, [μ-H**1**$^{\mathbf{NH}}$]$^+$	−1.86	[μ-H**1**$^{\mathbf{NH}}$]$^{+/0}$	1.19
$[Fe_2(adt^{NH2})(\mu\text{-H})(CO)_2(dppv)_2]^{2+}$, [μ-H**1**$^{\mathbf{NH2}}$]$^{2+}$	−1.77	[μ-H**1**$^{\mathbf{NH2}}$]$^{2+/+}$	1.00
$[HFe_2(pdt)(CO)_2(dppv)_2]^+$, [*t*-H**2**]+	−1.67	[*t*-H**2**]$^{+/0}$	2.56
$[Fe_2(pdt)(\mu H)(CO)_2(dppv)_2]^+$,[μ-H**2**]$^+$	−1.8	[μ-H**2**]$^{+/0}$	1.07

Table 4

Selected Electrocatalytic Properties of Protonated Derivatives of **1** and **2**.

Catalyst	Acid	Linear Region [H^+](mM)	Plateau Region [H^+] (mM)	$(i_c/i_p)_{max}$ [a]	k (s^{-1})	E_{cat} [b] (V vs $Fc^{+/0}$)	Overpotential [c] (V)
$[HFe_2(adt^{NH})(CO)_2(dppv)_2]^+$, $[t\text{-}H\mathbf{1}^{NH}]^+$	$ClCH_2CO_2H$	50–400	600–1200	69	5000	−1.49	0.71
$HFe_2(adt^{NH}H)(CO)_2(dppv)_2]^{2+}$, $[t\text{-}H\mathbf{1}^{NH2}]^{2+}$	CF_3CO_2H	20–280	370–750	167	58000	−1.11	0.51
$[Fe_2(adt^{NH})(\mu\text{-}H)(CO)_2(dppv)_2^+$, $[\mu\text{-}H\mathbf{1}^{NH}]^+$	$ClCH_2CO_2H$	2–50	60–90	10	20	−1.72	0.90
$[HFe_2(pdt)(CO)_2(dppv)_2]^+$, $[t\text{-}H\mathbf{2}]^+$	$HBF_4{\bullet}Et_2O$	1–8	10–20	5	5	−1.49	1.32
$[Fe_2(pdt)(\mu\text{-}H)(CO)_2(dppv)_2]^+$, $[\mu\text{-}H\mathbf{2}]^+$	$ClCH_2CO_2H$	2–10	14–40	3.5	3	−1.78	0.95

[a] i_c is the average catalytic current in the plateau region

[b] E_{cat} was calculated at each acid concentration in the linear region by the method described by Fourmond, *et al.*, considering the effects of homoconjugation for the two carboxylic acids.37 The E_{cat} values listed are averages from each acid concentration in the linear region.

[c] Overpotential = E^O HA/H2 - E_{cat}, where E^OHA/H2 is the standard reduction potential of the acid.37